P-101 Solid State NMR Study on Microbial Poly(ε-L-lysine) / Carboxymethyl Cellulose Blend Films and Hydrogels

Shiro Maeda[1], Mina Kobayashi[1], Kumiko Kato[1], and Ko-Ki Kunimoto[2]
[1]Division of Applied Chemistry and Biotechnology, Graduate School of Engineering, University of Fukui, Bunkyo, Fukui 910-8507, Japan
[2]Division of Material Engineering, Graduate School of Natural Science and Technology, Kanazawa University, Kakuma-machi, Kanazawa 920-1192, Japan

ABSTRACT
The hydrogels of microbial poly(ε-L-lysine)/carboxymethyl cellulose sodium salt (ε-PL/CMC) blends were investigated by using IR and solid-state NMR. ε-PL/CMC hydrogels were formed by bubbling carbon dioxide gas through ε-PL and CMC aqueous solution mixture. Formation of ε-PL/CMC hydrogel depends on composition ratio of ε-PL and CMC. Carbamate formation of amino groups of ε-PL by bubbling carbon dioxide gas through its aqueous solution and its reversibility to regenerate amino groups by bubbling nitrogen gas through it were also examined.

INTRODUCTION
Poly(ε-L-lysine) (ε-PL) (Scheme 1) is one of a few poly(amino acid)s which are known to occur in nature. Microbial ε-PL is a product of a variant of *Streptomyces albulus*. In ε-PL molecules, the ε-amino group of a L-lysine unit is linked to the α-carboxyl group of the other to form a peptide bond, leaving the α-amino group as a side chain. In recent years, there has been considerable interest in biopolymers because of concern over the environmental impacts arising from the disposal of petroleum based plastics. ε-PL is water soluble, biodegradable, edible and non-toxic toward humans and the environment, in addition to having broad-spectrum antibacterial activity. Thus, ε-PL and its derivatives have been of great interest for a broad range of industrial and biomedical applications. We have studied the molecular structure and the conformation of ε-PL in aqueous solution by pH dependent IR, circular dichroism, and ^{1}H and ^{13}C solution NMR.[1-3] Polymer blends are widely used as a means of tailoring and modifying characteristics of polymeric materials for various industrial and biomedical applications. A few studies on ε-PL based polymer blends have been reported. [5,6] We had reported characterization of several kinds of polymer blends of ε-PL. [4] Recently, we found that α-NH_2 groups of basic aqueous solution of ε-PL react with atmospheric CO_2 to make carbamate groups, -$NHCOO^-$.[7] Formation of carbamates is a characteristic found in ε-PL cast from basic aqueous solution exposed to the air or gaseous CO_2. It is not observed in ε-PL cast from acidic aqueous solution and ε-PL cast from degassed aqueous solution under CO_2 free environment. The carbonyl carbon and amide nitrogen of carbamate group appear at 164 ppm in ^{13}C spectrum and 92 ppm in ^{15}N spectrum, respectively. In addition to these peaks a peak always appears at 171 ppm in ^{13}C spectrum. We attributed this peak to the amide C=O carbon adjacent to the carbamated α-amino group. Bulky carbamate groups close to the C=O groups prevent formation of intermolecular hydrogen bonds and destruction of hydrogen bondings caused upfield shifts.

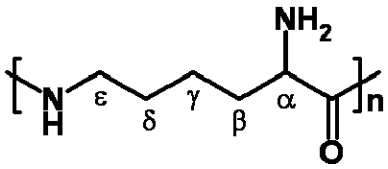

Scheme 1. Repeating units of poly(ε-L-lysine) (ε-PL).

Microbial Polymer, Poly(ε-L-lysine), Solid-state NMR.

Thus, peak area of carbamate carbonyl carbon at 164 ppm divided by sum of peak area of the peak at 178 ppm and that of 171ppm corresponds to the ratio of formation of carbamates. In this work, ε-PL/CMC hydrogels were formed by bubbling carbon dioxide gas into ε-PL and CMC aqueous solution mixture and structural analysis of them was carried out by IR and solid-state NMR measurements. Time dependence of the carbamate formation of ε-PL by bubbling carbon dioxide gas through its aqueous solution and its reversibility to regenerate amino groups by bubbling nitrogen gas through it were also examined.

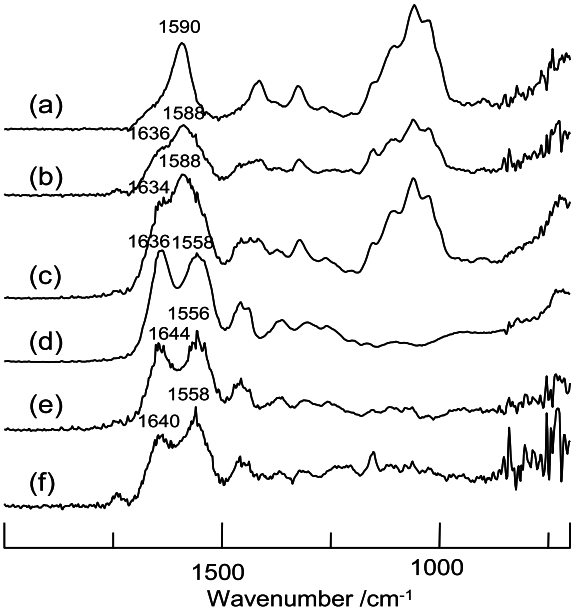

Figure 1. IR spectra of (a)CMC, ε-PL/CMC blend films of (b)1/1 and (c)2/1, (d) ε-PL film cast from aqueous solution, (e)[ε-PL/CMC=2/1]–[CMC] and (f)[ε-PL/CMC=1/1]– [CMC].

EXPERIMENTAL

Materials

Microbial poly(ε-L-lysine) (free form, ε-PL) was kindly supplied to us by Chisso Corporation. The number-averaged molecular weight of ε-PL was 4,090, which corresponds to the degree of polymerization of 32 based on the unit molecular weight of 128. Carboxymethyl cellulose sodium salt with average molecular weight of 500 was purchased from Tokyo Chemical Industry Co., and other reagents were purchased from Wako Pure Chemicals Co. and used without further purification. Ultra pure water, prepared by a Milli-QPlus ultra-pure water system (Millipore, USA) was used throughout the experiment. Carbon dioxide gas (200 mL/min) was supplied from liquid carbon dioxide cylinder.

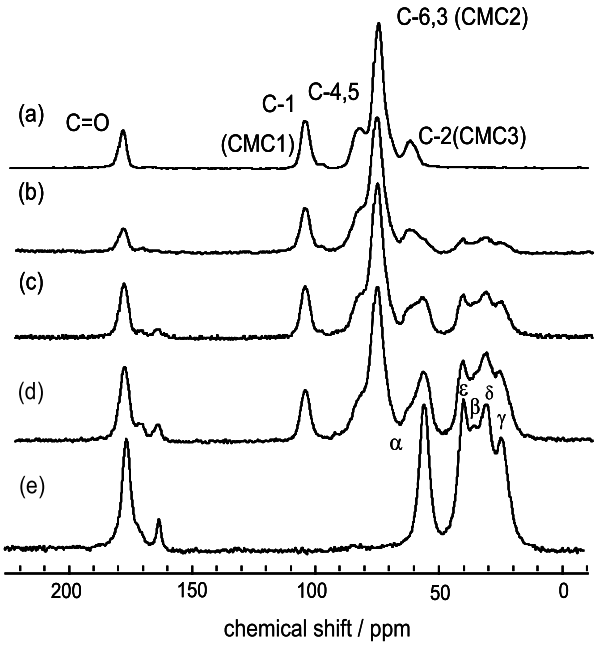

Figure. 2. ^{13}C CPMAS NMR spectra of (a) CMC cast film from aqueous solution, ε-PL/CMC blend films; (b) 1/2, (c) 1/1 and (d) 2/1, and (e) ε-PL cast film from aqueous solution.

Sample Preparation

ε-PL/CMC cast film was prepared as follows. ε-PL and CMC were separately dissolved in water (1.7 wt%) and stirred for one hour. The ε-PL and CMC aqueous solutions were mixed with different compositions of ε-PL/CMC: (a) 1/2, (b) 1/1, and (c) 3/1 in a unit molar ratio, and stirred one hour. This solution was cast on a Teflon petri dish and dried in the air for three days, and then dried in vacuum for two days at ambient temperature.[4] ε-PL/CMC hydrogel was prepared as follows. The ε-PL and CMC aqueous solutions (1.7 wt%) were separately prepared and mixed with various composition of ε-PL/CMC=2/1, 1/1, and 1/2 in a unit molar ratio. CO_2 gas (200 mL/min) was bubbled through a stirred ε-PL/CMC mixed aqueous solution in a glass vial at room temperature.

NMR Measurements

^{13}C CPMAS NMR spectra were measured with Chemagnetics CMX Infinity 300 operating at 75.6 MHz at room temperature. The samples were contained in a cylindrical rotor of zirconia ceramic. The rotor diameter was 5 mm, and spun at 7.0 kHz. Contact time was 1ms, and repetition time was 1 sec. The number of accumulation was about 10,000. ^{13}C signal of methyl carbon of hexamethylbenzene was externally referenced to 17.35 ppm from tetramethylsilane.

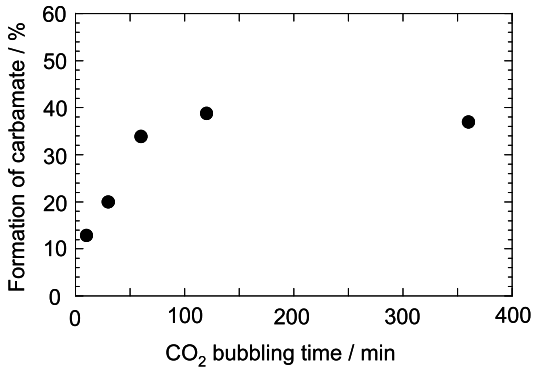

Figure 3. Formation of carbamate by CO_2 gas bubbling through a ε-PL aqueous solution.

RESULTS AND DISCUSSION

Figure 1 shows IR spectra of ε-PL and CMC cast from aqueous solution, and ε-PL/CMC blend films. [4] Since ε-PL has no absorption between 700 and 1300 cm^{-1}, IR spectrum of CMC was subtracted from that of blend film so that this region has no absorption to reveal the spectrum of ε-PL component of blend film (Fig. 1(e) and (f)). Peaks of 1636 and 1558 cm^{-1} are assigned to the amide I and amide II of ε-PL, respectively. In contrast hydrochloric salt form of ε-PL shows the amide I peak at 1670 cm^{-1}. The amide I and II frequencies of ε-PL components of the blend film are close to that of ε-PL. Therefore, α-NH_2 groups of ε-PL in blend films are not protonated and there is no electrostatic interaction between ε-PL and CMC. ^{13}C NMR spectra of ε-PL and CMC cast from aqueous solution, and ε-PL/CMC blend films are shown in Figure 2.[4] The blend films of ε-PL/CMC are transparent and flexible. Main chain amide carbonyl carbons of ε-PL appear at 178 ppm which show down field shift due to intermolecular hydrogen bondings.

Recently, we found that α-NH_2 groups of basic aqueous solution of ε-PL react with atmospheric CO_2 to make carbamate groups, -$NHCOO^-$.[7] The carbonyl carbon of carbamates appears at 164 ppm. In addition to this peak a peak at 171 ppm appears. We assigned it to amide C=O carbons which can not make intermolecular hydrogen bondings since there exist bulky carbamates groups close to these C=O groups. Thus, peak area of carbamate carbonyl carbon divided by sum of peak area of 178 ppm and that of 171ppm corresponds to the ratio of formation of carbamates. In Figure 3 this ratio is plotted against CO_2 bubbling (200mL/min) times. Figure 4 shows plots of pH value of ε-PL aqueous solution against CO_2 bubbling (200mL/min) time. pH value of ε-PL aqueous solution reduced rapidly and reached equilibrium value of 6.4 within 2 min. Figure 5 shows plots of pH value of ε-PL aqueous solution against N_2 bubbling (200mL/min) time after CO_2 bubbling

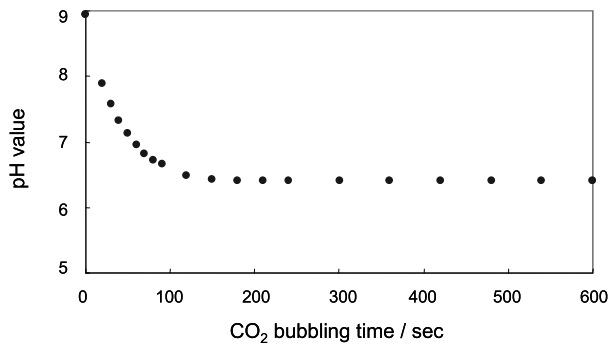

Figure 4. Plots of pH value of ε-PL aqueous solution against CO_2 bubbling (200mL/min) time.

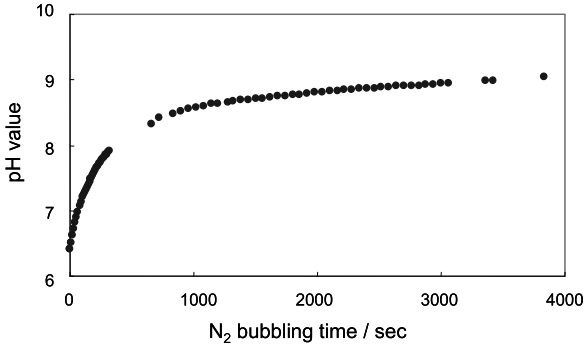

Figure 5. Plots of pH value of ε-PL aqueous solution against N_2 bubbling (200mL/min) time after CO_2 bubbling (200mL/min) of 30 min.

(200mL/min) of 30 min. pH value of ε-PL aqueous solution increased gradually and reached equilibrium value of 8.9 after about 1 hr. Reversibility of formation of carbamates of ε-PL was examined (Fig. 6): The obtained carbamates could release CO_2 at 333 K through N_2 gas bubbling of 1hr to regenerate the original ε-PL.

Figure 7 shows ^{13}C CPMAS NMR spectra of ε-PL/CMC=1/1 hydrogel.[8] When CO_2 gas was bubbled through ε-PL/CMC mixed aqueous solution, a pale green-yellowish precipitate was formed immediately. The reaction stopped within about 5 minutes and no more precipitate appeared. This may be a reason why a carbamate peak at 164 ppm is weak. In contrast to ε-PL/CMC cast films, there appears a strong peak at 171 ppm in hydrogel. This is not a peak observed in carbamated ε-PL because intensity of a peak at 164 ppm is very weak. We think that α-NH_2 groups of ε-PL were protonated through CO_2 bubbling and there may be electrostatic interaction between ε-PL-NH_3^+ and CMC-COO^- to make insoluble hydrogel. Peaks at 171 and 178 ppm can be assigned to carbonyl carbon of ε-PL and CMC, respectively.

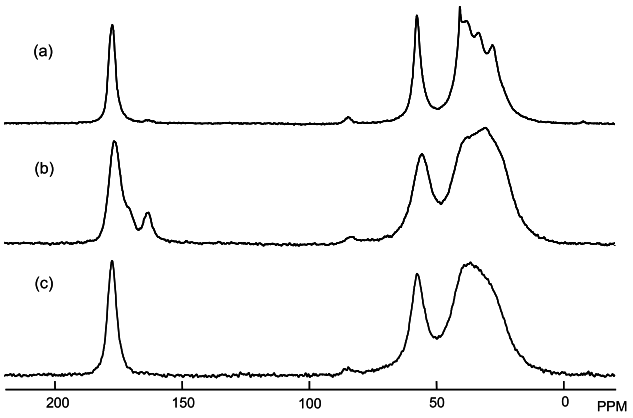

Figure 6. ^{13}C CPMAS NMR spectra of ε-PL films cast from aqueous solution. Conditions: (a) under CO_2 free environment; (b) 30 min CO_2 bubbling (200mL/min); (c) 1 hr N_2 bubbling (200mL/min) at 333 K after CO_2 bubbling of 30 min.

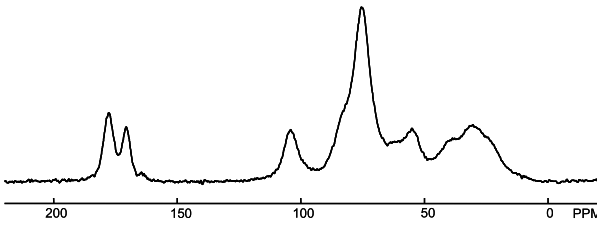

Figure 7. ^{13}C CPMAS NMR spectrum of ε-PL/CMC=1/1 hydrogel.

REFERENCES

1. S. Maeda, C, Sasaki, and K.-K. Kunimoto, in *NMR Spectroscopy of Polymers: Innovative NMR Strategies for Complex Macromolecular Systems*, ACS Symposium Series, Ed. H. N. Cheng (American Chemical Society), in press (2011).
2. S. Maeda, T. Mori, K.-K. Kunimoto, and C. Sasaki, *Kobunshi Kako*, **52**, 516-522 (2003).
3. S. Maeda and K.-K. Kunimoto, *Chemical Engineering*, **56**, 719-724 (Kagaku Kogyosha, Inc., Japan) (2011).
4. S. Maeda, Y. Fujiwara, K. Kato, and K.-K. Kunimoto, *Polymer Preprints* , 49, 730-731 (2008).
5. T. Ichikawa, Y. Mitsumura, and T. Nakajima, *J. Appl. Polym. Sci.*, **54**, 105-112 (1994).
6. A. Asano, Y. Murata, and T. Kurotsu, *e-J. Soft Mater.*, **3**, 1-8 (2007).
7. S. Maeda, S. Oumae, S. Kaneko, and K.-K. Kunimoto, *Polym. Bull.*, in press (2011).
8. S. Maeda, K. Takagi, M. Kobayashi, and K.-K. Kunimoto, *submitted for publication*.

P-102 Characterization of microbial poly(γ-glutamic acid)s with different D/L ratio by solid NMR

Shiro Maeda, Shingo Oumae, and Kazumasa Oiwa
Division of Applied Chemistry and Biotechnology, Graduate School of Engineering, University of Fukui, Bunkyo, Fukui 910-8507, Japan

ABSTRACT
Characterization of microbial poly(γ-glutamic acid)s (γ-PGA) with different D/L ratio was done by using solid NMR. Free form (acid form) of γ-PGA shows a characteristic peak at 171ppm in ^{13}C solid NMR spectrum and a strong absorption band at 1735 cm^{-1} in IR spectrum which are not observed in its sodium salt, γ-PGA/Na. IR and ^{13}C solid NMR spectra of three kinds of PGA samples precipitated from acidic aqueous solution of γ-PGA/Na with different D/L ratio, 8:2, 7:3, and 5:5 were measured. There appeared a peak at 171 ppm in ^{13}C solid NMR spectra and a absorption band at 1735 cm^{-1} in IR spectra of precipitates. The intensities of peak at 171ppm were close to each other. According to these results, it was concluded that this peak is not characteristic of D-form or L-form.

INTRODUCTION
Poly(γ-glutamic acid) （γ-PGA） (schem1) is one of a few poly(amino acid)s which are known to occur in nature. We had reported on characterization of γ-PGA, γ-PGA sodium salt (γ-PGA/Na), γ-PGA films cast from aqueous solution of various pHs, and polymer blend films with poly(vinyl alcohol) (PVA) done by using solid-state NMR and IR spectroscopies. We found that free form (acid form) of γ-PGA shows a characteristic peak at 171ppm in ^{13}C solid NMR spectrum and a strong absorption band at 1735 cm^{-1} in IR spectrum which are not observed in its sodium salt, γ-PGA/Na.

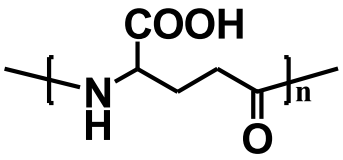

Scheme 1. Repeating units of poly(γ-glutamic acid) (γ-PGA).

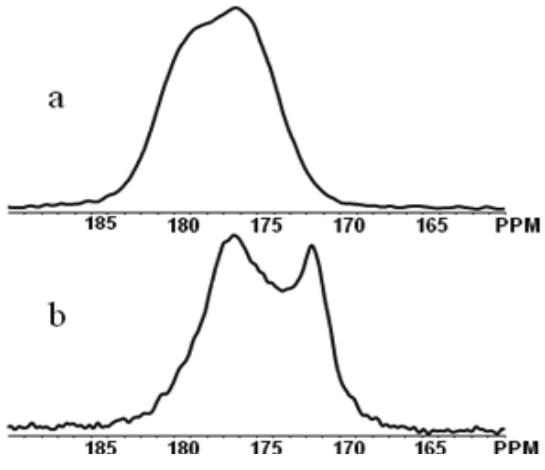

Figure 1. Carbonyl carbon region of ^{13}C NMR spectra of sample 2 (γ-PGA/Na); (a) raw material and (b) precipitate from acidic aqueous solution.

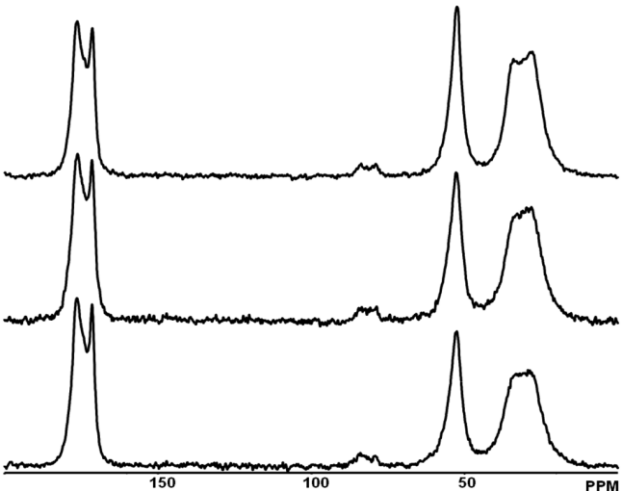

Figure 2. ^{13}C NMR spectra of precipitates from acidic aqueous solution; (a)sample 1, (b)sample 2, and (c)sample 3.

Microbial Polymer, poly(γ-glutamic acid), Solid-state NMR.

EXPERIMENTAL

Materials

Sample 1 of γ-PGA salt was kindly donated from Ajinomoto Co., Inc. D/L ratio of Sample 1 is 8:3. Sample 2 of γ-PGA/Na was purchased from Wako Pure Chemicals. Mn of sample 2 is between 200000 and 500000, and D/L ratio is 7:3. Sample 3 of γ-PGA salt was kindly donated from Yakult Pharmaceutical Industry Co., Ltd. D/L ratio of Sample 3 is 5:5. Samples were used without further purification.

Sample Preparation

1M HCl aqueous solution was added to the aqueous solutions of γ-PGA to adjust the pH of the solution to about pH 1. Precipitation had gradually appeared by standing the solution for several days. The precipitate was taken out by centrifugation and dried under vacuum for two days.

NMR Measurements

^{13}C CPMAS NMR spectra were measured with Chemagnetics CMX Infinity 300 operating at 75.6 MHz at room temperature. The samples of a cast film cut into small pieces with scissors or in powder form were contained in a cylindrical rotor of zirconia ceramic. The rotor diameter was 5mm, and the rotor was spun at 7.0 kHz. Contact time was 1ms, and repetition time was 1 sec. The number of accumulation was about 10000 for ^{13}C. ^{13}C signal of methyl carbon of hexamethylbenzene was externally referenced to 17.35 ppm from tetramethylsilane.

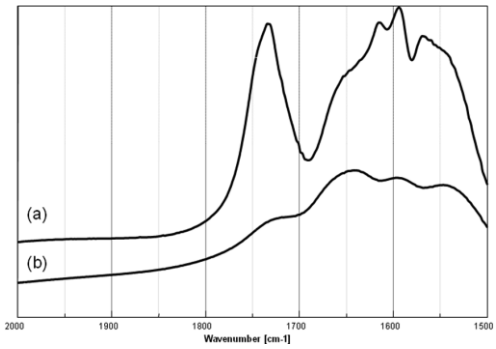

Figure 3. IR spectrum of sample 1. (a) precipitate from acidic aqueous solution and (b) raw material.

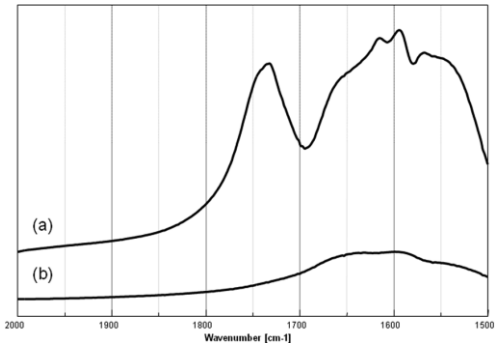

Figure 4. IR spectrum of sample 2. (a) precipitate from acidic aqueous solution and (b) raw material.

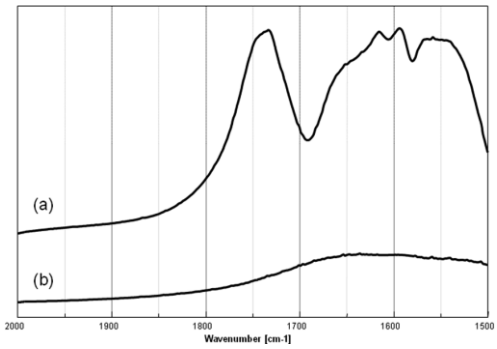

Figure 5. IR spectrum of sample 3. (a) precipitate from acidic aqueous solution and (b) raw material.

RESULTS AND DISCUSSION

Figure 1 shows carbonyl carbon region of ^{13}C NMR spectrum of sample 2. ^{13}C NMR spectrum of precipitate from acidic aqueous solution (Figure 1b) is the same as that of γ-PGA, and we identified the precipitate with γ-PGA. Figure2 shows ^{13}C NMR spectra of precipitates of three samples. They resemble each other in spectral profile regardless of difference in D/L ratio. Figures 3-5 show IR spectra of (a) precipitate from acidic aqueous solution and (b) raw material for samples 1-3, respectively. In IR spectra of precipitates of all samples, there appeared a peak of 1735cm^{-1} that do not appear in that of raw material. This peak is assigned to dimeric form of carboxyl group. According to these results, it was concluded that the peak at 171ppm in ^{13}C NMR spectrum is not characteristic of D-form or L-form of γ-PGA.

REFERENCES

1. S. Maeda, *et al.*, *Polym. Preprints, Jpn.* 57(2), 3300(2008) ; *Proceedings of the 47th Annual Meeting of The Magnetic Resonance Society of Japan*, 302-303(2008) ; *Polym. Preprints, Jpn.* 58(1),1162(2009) ; *ibid.* 58(2), 3394(2009) ; *ibid.* 59(1),1060(2010).

P-103 Reorientational motion of BD_4 ion in $LiBD_4$ as studied by solid-state NMR

Keiko Jimura, Shigenobu Hayashi
Research Institute of Instrumentation Frontier, National Institute of Advanced Industrial Science and Technology (AIST)

ABSTRACT

It is well known that the BH_4 anions undergo fast reorientational motion at room temperature in metal borohydride (MBH_4). We have studied the motion by means of solid–state NMR. The motion is isotropic in $NaBH_4$ and KBH_4. On the other hand, two types of reorientational motion take place in $LiBH_4$ (orthorhombic phase). In the present work, we focus on the ion dynamics in $LiBD_4$ (orthorhombic phase). The ^2H spin-lattice relaxation times (T_1) were analyzed in detail, and the motional mode is discussed through the effective quadrupole coupling constant obtained by the analysis. The line shapes of the ^2H static NMR spectra were also analyzed by theoretical simulation.

Experiments

$LiBD_4$ (95 atom% D) was purchased from Sigma-Aldrich. It was sealed in a Pyrex grass tube under vacuum. The ^2H static NMR spectra were measured with Bruker ASX200 at the Larmor frequency of 30.72 MHz in the temperature range between 135 and 440 K. A Bruker broadband probehead with a solenoid coil was used. The quadrupole echo pulse sequence ($\pi/2–\tau_1–\pi/2–\tau_2$-echo) was used to trace the spectra and the latter half of the echo signal was Fourier-transformed. The inversion recovery pulse sequence ($\pi–\tau–\pi/2–\tau_1-\pi/2–\tau_2$-echo) and the saturation recovery pulse sequence ($(\pi/2–\tau_3)_n–\tau–\pi/2–\tau_1-\pi/2–\tau_2$-echo) were used for the T_1 measurements. The spectra whose line shape was modulated by molecular motions were simulated by MXET1 program installed in a personal computer.

Results and discussion

Figure 1 shows several ^2H static NMR spectra of $LiBD_4$. At about 380 K, $LiBD_4$ undergoes a structural transition from orthorhombic (low temperature phase; LT) to hexagonal (high temperature phase; HT). The obtained spectra consisted of only one relatively sharp peak in LT phase. The line width was about 5.6 kHz at 140 K. In the temperature region below 180 K, the line width gradually increased with increase in temperature. It was about 6.4 kHz at 180 K. Above 180 K, it gradually decreased with increase in temperature. In HT phase, Pake doublet splitting which is characteristic in ^2H static NMR spectra was observed. At 440 K, the line width was about 1 kHz and the split width was about 0.9 kHz.

These results demonstrate that the tetrahedral BD_4 anions reorient very fast in LT phase. The reorientation doesn't stop even at 140 K. The motion is not an ideal isotropic rotation. The observed spectra are simulated theoretically, and the anisotropic property of the BD_4 rotation will be discussed in detail.

Figure 2 shows the T_1 values of $LiBD_4$ measured at 30.72 MHz. The temperature dependence of the ^2H T_1 values shows the similar tendency to that of the ^1H T_1 values in $LiBH_4$. At about 380 K, $LiBD_4$ undergoes a structural transition from LT to HT phases, and the ^2H T_1 value changes discontinuously.

Solid-state NMR, Hydrogen storage material, Borohydrides

The observed ^{2}H T_1 curve in LT phase consists of two components. They have T_1 minima at about 190 and 200 K. The presence of two components indicates that two independent rotations of the BD_4 ion take place. The T_1 minimum values are important information for the BD_4 motion. The values reflect both the dipole-dipole interactions with surrounding spins and the quadrupole interaction averaged by the motion. The change from a rigid state to a state under an anisotropic rotation results in the local T_1 minimum on the lower-temperature side. The local T_1 minimum on the higher-temperature side is originated from a state change from the anisotropic rotation to an isotropic-like rotation.

The temperature dependence of the T_1 values is analyzed theoretically according to the theory of Bloembergen-Purcell-Point (BPP) on the condition that $LiBD_4$ (LT) has two independent rotations. Two anisotropic BH_4 rotations are assumed; jump rotations around a 3-fold axis and a 2-fold axis. The motional mode will be discussed through the effective quadrupole coupling constant obtained by the analysis.

Acknowledgments

This work was supported by The New Energy and Industrial Technology Development Organization (NEDO) under "Advanced Fundamental Reseach on Hydrogen Storage Materials (Hydro-Star)"

Reference

[1] K. Jimura and S. Hayashi, The 49th Annual Meeting of the NMR society Japan (2010).

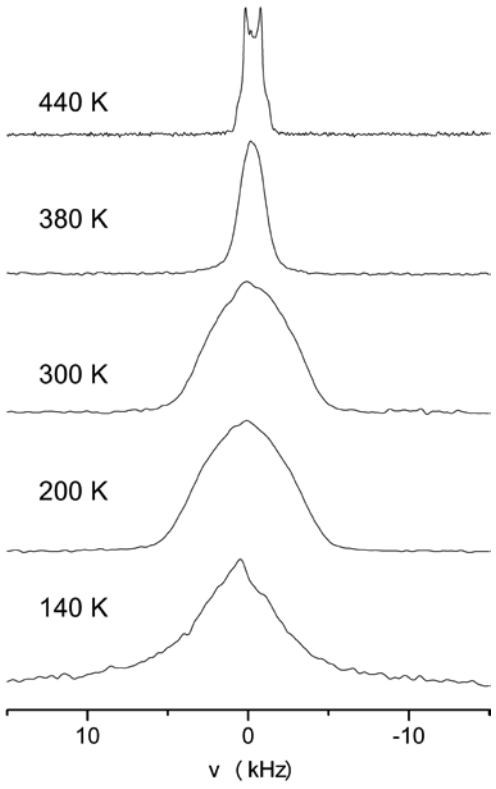

Fig. 1. ^{2}H static NMR spectra of $LiBD_4$

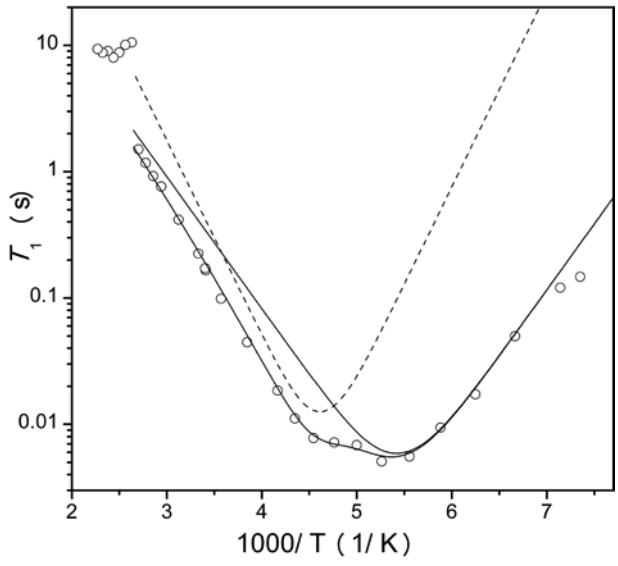

Fig. 2. ^{2}H T_1 of $LiBD_4$ (30.72 MHz)

P-104 Alkali effects on structure and viscosity in R_2O (R=Li, Na, K, Rb, Cs)-CaO-Al_2O_3-SiO_2 glasses and melts

Koji Kanehashi[1], Yuta Shimamura[2] and Sohei Sukenaga[2]
[1]Advanced Technology Research Laboratories, Nippon Steel Corporation
[2]Department of Material Science and Engineering, Kyushu University

Abstract

Microscopic chemical structures of R_2O (R=Li, Na, K, Rb, Cs)-CaO-Al_2O_3-SiO_2 glasses have been investigated by solid-state ^{29}Si and ^{27}Al NMR and the relationship between structure and viscosity has been studied. ^{27}Al MAS NMR spectra proves increase in the mean coordination number around Al with decreasing the ionic radius of alkali (Li<Na<K<Rb<Cs). Macroscopic viscosities of R_2O-CaO-Al_2O_3-SiO_2 melts are low in the order of the ionic size from smallest (Li) to largest (Cs) at the same temperature. From these results, pentacoordinated Al (higher coordination number) might act as intermediates of viscous flow.

Silicate and aluminosilicate melts are major components in many geological processes in the Earth's mantle and crust. They also are important in industrial processes, e.g. for glass making and as slags in metal extraction from ores. Because macroscopic physical and chemical properties of these materials are controlled by processes at the microscopic level, it is important to obtain atomic-scale information on both structure and dynamics.

The calcium aluminosilicate (CAS) system is one of the most significant ternary systems because of its extensive use in industry, by virtue of the excellent chemical, mechanical and optical properties of CAS and related glasses. Alkali and alkali-earth cations added to CAS systems play important role to control macroscopic properties (e.g. viscosity and liquidus temperature). In the present study, we report solid-state ^{29}Si and ^{27}Al NMR experiments to investigate structure and dynamics of Si^{4+} and Al^{3+} ions in a CAS glass. The relationship between microscopic structure and macroscopic viscous flow are also discussed.

The CAS glass and melt studied here contain 14 mol% R_2O (R=Li, Na, K, Rb, Cs), 38 mol% CaO, 2 mol% Al_2O_3 and 46 mol% SiO_2. Two non-bridging oxygens per tetrahedral SiO_2 or AlO_4 unit exist in these compositions. The glass was synthesized from reagent-grade, well-dried starting materials, R_2CO_3, $CaCO_3$, Al_2O_3, and ^{29}Si-enriched (98.8 %) SiO_2 in air in a Pt crucible using the conventional melt quenching method (quenching the crucible in water) at 1550 °C for 1 hour.

^{29}Si and ^{27}Al MAS NMR data were collected using Varian/Chemagnetics CMX 300 (7.0 T) and JEOL ECA 700 (16.4 T) spectrometers at Larmor frequencies of 59.55 and 182.31 MHz, respectively. A Varian/Chemagnetics 4 mm MAS probe were used with spinning rates of 16 kHz for ^{29}Si spectra, and a JEOL 4 mm MAS probe with 18 kHz spinning for ^{27}Al spectra. Pulse recycle delays were long enough to allow full relaxation. ^{29}Si and ^{27}Al chemical shifts were referenced to an external polydimethylsilane (-34 ppm) and an external 0.1 M aqueous aluminum chloride solution (-0.1 ppm), respectively. Centers of gravity for MAS spectra were determined by integration.

The crucible filled with slag powder was placed in a crucible supporter in the furnace and heated up to 1600 °C. After then, the molten slag was kept at that temperature until the detected

glass and melt, solid-state ^{29}Si and ^{27}Al NMR, viscosity

voltage value (viscosity) became constant. An apparent viscosity was calculated based on the reference relationship between the viscosity and the potential difference, which was obtained by using various silicone oils beforehand.

The ^{29}Si line shape was a single, featureless peak in all ^{29}Si MAS spectra for 14 R_2O-38 CaO-2 Al_2O_3 and-46 SiO_2 glasses. Four-coordinated Si ($^{[4]}$Si) signals were only observed. Five ($^{[5]}$Si) and six-coordinated ($^{[6]}$Si) generally show Si peaks around -150 and -200 ppm, respectively[1]. There was no signals in this frequency regions, which prove no $^{[5]}$Si and $^{[6]}$Si in the present glasses.

Peak positions (centers of gravity) shift to lower frequency with increasing cationic size of R except for R=Na in which very small (0.1 ppm) shifts to high frequency observed compared to R=Li. Line width in Figure 1 increase with increasing cationic size, indicating larger dispersion in chemical shifts. For example, since Cs^+ ion is about three times larger than Li^+ ion, Cs^+ ions inside clusters might easily distort SiO_4 tetrahedra, which causes distributions of Si-O bond lengths and O-Si-O bond angles.

^{27}Al MAS spectra for 14 R_2O-38 CaO-2 Al_2O_3 and-46 SiO_2 glasses are shown in Figure 1. Pentacoordinated ($^{[5]}$Al) and octahedral Al ($^{[6]}$Al) were clearly resolved for R=Li. Since the present sample is in the percalcic region ((CaO+R_2O)/Al_2O_3>1), there are enough Ca^{2+} and R^+ ions to charge-compensate the $(AlO_4)^-$ tetrahedra. Therefore, most Al atoms occur in tetrahedral sites with a small proportion of pentacoordinated and octahedral sites. A small proportion of $^{[5]}$Al occur for R=Na, which was demonstrated by an ^{27}Al 3QMAS experiment. On the other hand, $^{[5]}$Al signals are below noise levels for R=K, Rb, Cs.

At the same temperature above liquidus, e.g. 1500 °C, the viscosity decreases with decreasing the ionic size of R (Figure 2). Break point (temperature at which the viscosity drastically changes) also decreases in the order of the ionic size from smallest (Li) to highest (Cs). Thus, melts become more mobile with smaller cations.

From these results, a pentacoordinated intermediate state (AlO_5) might allow for chemical exchange of aluminum environments[2]. The fact that the pentacoordinated species exists even at T_g (glassy state) as seen in the ambient temperature MAS NMR spectra for R=Li and Na (Figure 1), supports this suggestion. We will present relaxation data for ^{29}Si and ^{27}Al on the day.

References
[1] K. J. D. Mackenzie, M. E. Smith, Multinuclear Soild-State NMR of Inorganic Materials. 1st ed. Oxford, Pergamon, 2002, p225.
[2] K. Kanehashi, J. F. Stebbins, *J. Non-Cyst. Solids.*, **353** (2007) 4001.

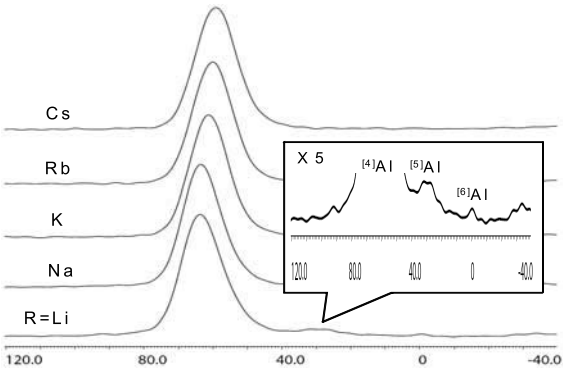

Figure 1 ^{27}Al MAS NMR spectra for 14 R_2O-38 CaO -2 Al_2O_3 and-46 SiO_2 glasses.

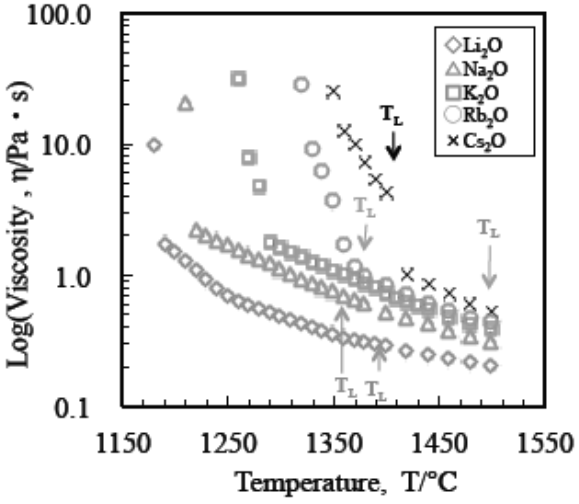

Figure 2 Temperature dependence of viscosities for 14 R_2O-38 CaO-2 Al_2O_3 and-46 SiO_2 melts. T_L denotes liquidus temperature.

P-105 Characterization of zeolite acid site by solid-state ^{1}H and ^{27}Al NMR spectroscopy in combination with NH_3-TPD

Mie Nayuki[1], Yasuhiro Hashimoto[1,2] Ryusuke Miyazaki[3], and Kenji Akagishi[3]
[1]Analysis & Simulation Center, Asahi Kasei Corporation
[2]Strategic Planning & Development, Asahi Kasei Corporation
[3]Catalyst Laboratory, Asahi Kasei chemicals Corporation

Introduction

Zeolite acidity is a pivotal property when functioning as catalysis. Thus, there have been a numerous studies to characterize the acid site structure, relating to their acid strength. The acidy is expressed by substituting silicon by aluminum atoms, forming the tetrahedral aluminum acidic site. Therefore, one-dimensional ^{27}Al solid state NMR has been conventionally applied where tetrahedral as well as octahedral aluminum signals are observed. Octahedral aluminum, extra-framework sites, has been regarded as non-active site. Another NMR approach is ^{1}H solid state NMR methods, which take advantage of directly observing the proton of Brønsted acid sites(1).

Even these effective NMR techniques, however, do not provide comprehensive structure information on the acid site structure because of the following reasons. (1) ^{1}H solid state NMR may detect only the Brønsted acid site, leaving the Lewis acid site undetected. (2) The Lewis acid site may not necessarily be a tetrahedral aluminum site.

Here, we present an attempt to characterize all the acid sites including Lewis acid sites as well as Brønsted sites by combined use of NH_3-TPD(2) and NMR. NH_3-TPD is a method generally used to characterize the acidic property of zeolites, where NH_3 is adsorbed onto all the acidic sites followed by a desorption procedure by raising the temperature. As desorption temperature of NH_3 is related to acidic strength, desorption profiles should represent the acidic strength property of the samples.

We conducted ^{1}H NMR analysis for the NH_3 adsorbed zeolite prepared by NH_3-TPD method, where acid detection was indirectly made by observing NH_3 proton. Not only did we successfully detect all the acid sites, but also selective acid detection according to their acid strength was possible by controlling the desorption temperature of NH_3-TPD. Further, by applying ^{27}Al-^{1}H HETCOR, the acid site aluminum structure information will possibly be obtained as well(3).

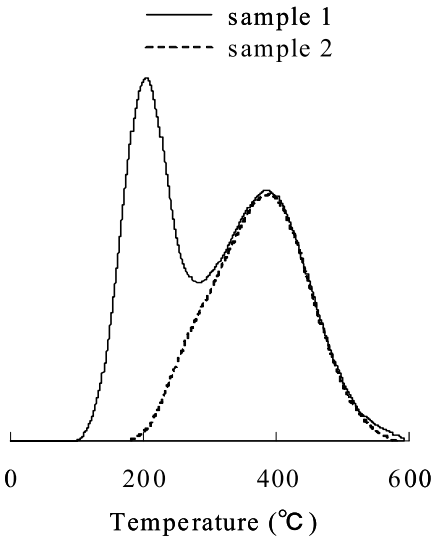

Figure 1. NH_3-TPD profiles of sample 1 and 2.

Experimental

H-MFI (SiO_2/Al_2O_3=27) was used as a blank sample. For the NH_3-TPD, TPD-1-ATw (BEL JAPAN.Inc) was used.

Zeolite, Solid NMR, NH_3-TPD

After adsorption of NH_3 onto zeolite sample, desorption was made by raising temperature appropriately. NMR measurements were conducted with JEOL ECA700 spectrometer with 18 kHz magic angle spinning. Both of one-dimensional ^1H and ^{27}Al N MR spectra were obtained by a single pulse method. For $^{27}Al\{^1H\}$CP HETCOR, 50us CP time was used. To prevent the adsorption of the water onto the NH_3-TPD prepared zeolite samples, NMR tube sampling was carried out in an argon glove box.

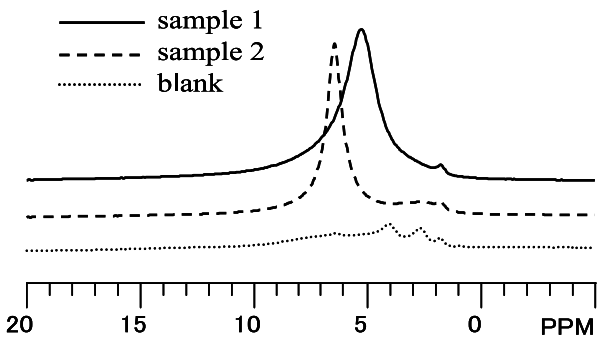

Figure 2. ^1H solid-state NMR spectra of NH_3 adsorbed (sample 1 and 2) and blank zeolites.

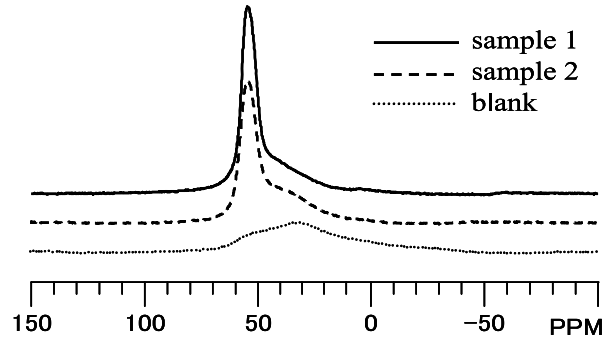

Figure 3. ^{27}Al solid-state NMR spectra of NH_3 adsorbed (sample 1 and 2) and blank zeolites

Results and Discussion

As Figure 1 shows selectively NH_3 adsorbed zeolite samples were obtained. In sample 1 all the acid site was NH_3 adsorbed, while the adsorption was made only onto strong acid site in sample 2.

NH_3 proton peaks were observed in ^1H NMR spectrum (Figure 2), where higher frequency shift was observed in sample 2. This should reflect the strong acidity in sample 2. In ^{27}Al NMR spectra, dramatic sharpening of tetrahedral signal by adsorption of NH_3 was observed. The sharpening confers the method significant advantages because ^{27}Al NMR of zeolites usually suffers from serious broadening without hydrations.

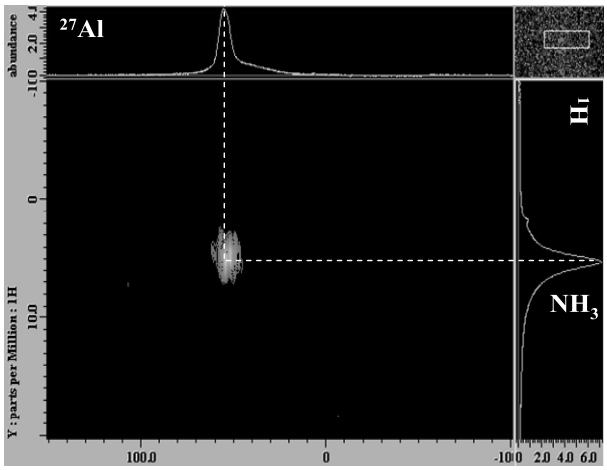

Figure 4. $^{27}Al\{^1H\}$CP Hetcor spectrum of sample 1.

A correlation peak was detected between NH_3 proton signal in ^1H NMR and tetrahedral aluminium signal in ^{27}Al NMR, suggesting the active aluminium sites. It is worth mentioning that only sharp tetrahedral aluminum signal shows correlation, which may possibly suggest not all the tetrahedral aluminium is necessarily the active acid site.

Thus, the NMR spectroscopy in combination with NH_3-TPD is promising method particularly for the detailed zeolite acid site structure analysis.

Reference

(1) J. Huang, et al., J. Phys. Chem. C, 112, 3811 (2008)
(2) M. Niwa, et al., Hyoumen Kagaku, 24, 635 (2003)
(3) Y. Hashimoto, 11-1 NMR Kenkyuukai proceedings, 9 (2011)

P-106 Surface acid property of zeolites studied by solid-state NMR

Natsuko Kojima, Shigenobu Hayashi

Research Institute of Instrumentation Frontier, National Institute of Advanced Industrial Science and Technology (AIST)

[Introduction]

Solid acid catalysts have intensively been studied, which can replace liquid acid catalysts. Evaluation of the acid properties is important in order to develop new acid catalysts. The acid properties have been studied by several techniques such as ammonia temperature-programmed desorption (NH_3-TPD), FT-IR and solid-state NMR. NMR is non-invasive and non-destructive. The NMR signal intensity is proportional to the atomic concentration and, thus, the obtained spectra are analyzed quantitatively. We can observe ^{1}H NMR signals of Brønsted acid sites directly with high sensitivity. In our previous work we studied acid properties of H-type mordenite by solid-state NMR [1]. The observed ^{1}H NMR signal contained a signal of H_2O adsorbed from atmosphere in the preparation process.

In the present work, we have studied acid properties of H-type ZSM-5 by solid-state NMR. Brønsted acid sites on H-type ZSM-5 is also very sensitive to H_2O in air atmosphere. We were very careful of avoiding H_2O adsorption from atmosphere. The sample preparation method was improved to avoid H_2O adsorption.

[Experimental]

The ZSM-5 zeolite samples were reference catalysts supplied by The Catalysis Society of Japan, which had been characterized by a number of methods. They were coded as follows: H-type ZSM-5 samples were JRC-Z5-25H, JRC-Z5-70H, and JRC-1000H. JRC meant Japan Reference Catalyst and Z was zeolite. H attached after the number meant H^+ form. The number was a nominal SiO_2/Al_2O_3 molar ratio. The three samples are named ZSM5-25H, ZSM5-70H, ZSM5-1000H in the present work. The as-supplied samples of ZSM5-25H and ZSM5-1000H contained NH_4^+ ions and, therefore, those samples were calcined at 808K under an air atmosphere to convert to H^+ form.

The samples were dehydrated as follows. The sample was packed in a glass tube with a stopcock. Then the tube was connected to a glass vacuum line and it was evacuated with a oil rotary vacuum pump. The sample temperature was increased up to 473K under evacuation and it was kept for three hours. The glass tube was left over night under static vacuum at room temperature. The samples were packed into a MAS rotor of a 4-mm diameter under an N_2 atmosphere. After packing into the rotor, the sealing of the 4-mm MAS rotor was rather good.

^{1}H MAS NMR spectra were measured at room temperature with a Bruker ASX400 spectrometer at Larmor frequency of 400.13 MHz. A Bruker MAS probehead was used with a zirconia rotor of a 4.0-mm outer diameter. The ordinary single-pulse sequence was used. The frequency scales of the ^{1}H spectra were expressed with respect to neat tetramethylsilane (TMS) by adjusting the ^{1}H singal of adamantane spinning at 8.0 kHz to 1.87 ppm. The ^{1}H NMR spectra were analyzed quantitatively by using adamantane as an external reference.

[Results and discussion]

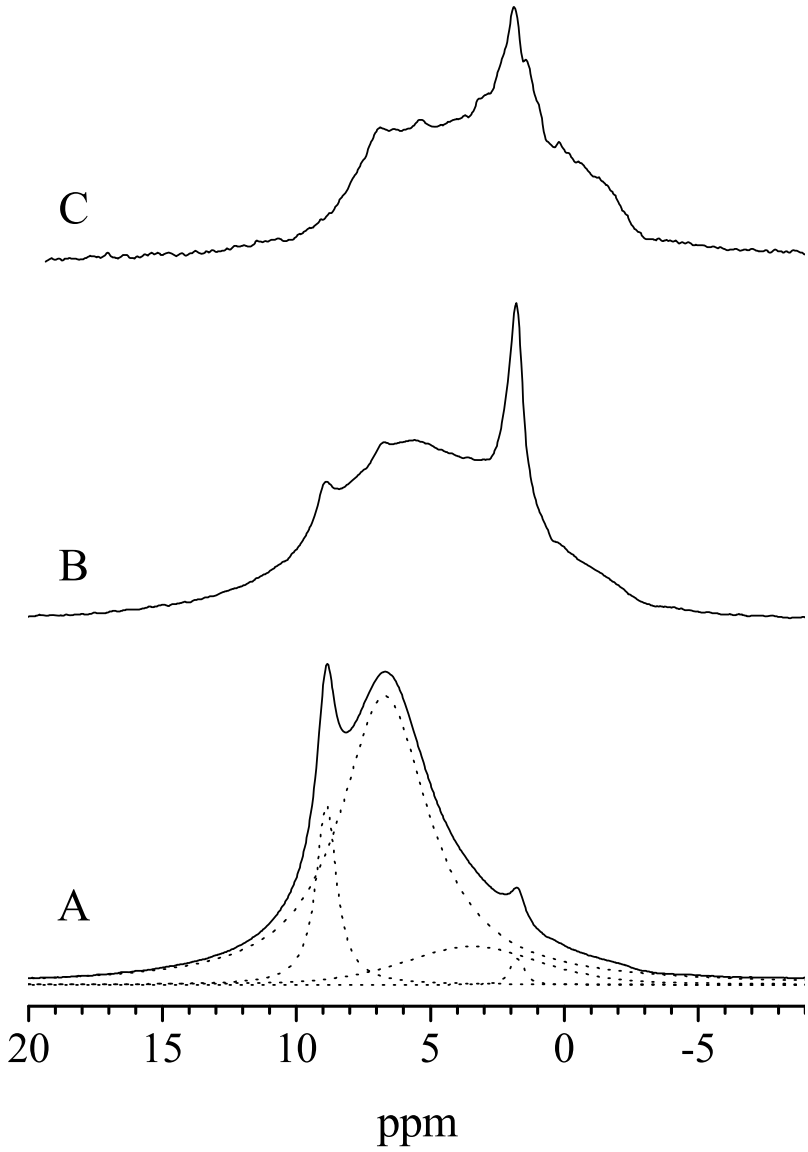

Figure 1. ^{1}H MAS NMR spectra of H-type ZSM5 after dehydration. (A) ZSM5-25H, (B) ZSM5-70H, and (C) ZSM5 -1000H. The spinning rate was 8 kHz. The spectrum of ZSM5 -25H consists of four components shown by chain lines.

Figure 1 shows ^{1}H MAS NMR spectra of H-type ZSM-5 after the dehydration process. The spectrum of ZSM5-25H consists of four components, which are centered at 8.88, 6.71, 3.43 and 1.76 ppm, as shown by chain lines in Fig. 1A. The 1.76-ppm component is ascribed to isolated Si-OH, the 8.88-ppm component to hydrogen-bonded Si-OH. The broad 3.43-ppm component is ascribed to OH groups attached to out-of-framework Al. The 6.71-ppm component is dominant, being ascribed to Brønsted acid sites. The spectra of ZSM5-70H (Fig. 1B) and ZSM5-1000H (Fig. 1C) are similarly deconvoluted to ZSM5-25H.

The ^{1}H NMR spectra were analyzed quantitatively, and the concentration of each component is evaluated. The ^{1}H chemical shift value of Brønsted acid sites reflect the acid strength, and we will discuss the acid strength and its amount.

[Acknowledgements]

This work was supported by Grant-in-Aid for Scientific Research (No. 23550236) from the Japanese Ministry of Education, Culture, Sports, Science and Technology.

[References]

[1] S. Hayashi, N. Kojima, Micropor. Mesopor. Mater., 141 (2011) 49.

Keywords : Solid acid catalysts, Zeolites, Surface property

P-107 Quantitative tracing of electrolyte ions in the EDLC system using solid-state NMR

Keiko Ideta[1], Yusuke Shingai[2], Masanori Saito[2], Jin Miyawaki[1], Isao Mochida[3] and Seong-ho Yoon[1,2]
[1]Institute for Materials Chemistry and Engineering, Kyushu Univ.
[2]Interdisciplinary Graduate School of Engineering Sciences, Kyushu Univ.
[3]Research and Education Center of Carbon Resource, Kyushu Univ.

1. Introduction

An electric double layer capacitor (EDLC) shows a high power density, fast charge and discharge rates, and a good cycling performance, thus, is expected as a new energy storage device. Porous carbon materials, such as activated carbons, have been often applied as an electrode material of EDLC, but KOH-activated carbons often give rise to higher capacitances as compared with steam-activated ones regardless of same surface area and pore size distribution. To further improve the EDLC performance, therefore, detailed understandings of charging and discharging behaviors and states of electrolyte ions in pores of the carbon electrode materials prepared by different activation methods are indispensable.

In this study, we quantitatively analyzed the electrolyte ion behaviors in the pores of KOH- and steam-activated carbons using ^{19}F solid-state NMR method to investigate correlations with the capacitance.

2. Experimental

Activated carbon was prepared from spherical phenol resin (S-BEAPS、Asahi Organic Chemicals Industry Co., Ltd.) by KOH or steam activation. The KOH- and steam-activated carbons were designated as SK and SH, respectively.

The disc-type electrodes were prepared by compressing the prepared activated carbons with PTFE as a binder and Ketjen black as a conductive substance. The weight ratios were 8:1:1. The electrodes were impregnated with the electrolyte solution 1 M Et_4NBF_4/PC under vacuum for 3 h. The two-electrode test cell was charged up to 2.7 V and then discharged to 0 V to measure the capacitance.

The ^{19}F solid-state NMR measurements were carried out for positive electrodes at charged or discharged state. A main peak of PTFE in each NMR spectrum was used as the internal standard for quantitative analysis.

3. Results and discussion

The BET surface area of the prepared activated carbons (SK and SH) is shown in Table 1 together with the capacitance. Both SK and SH were found to be mainly microporous. Although they had similar surface area and pore size distribution, SK showed higher capacitance than SH.

Fig. 1 shows ^{19}F solid-state NMR spectra of SK and SH at charged and discharged states. In all cases, two main peaks were observed. Sharp peaks observed at low magnetic field can be assigned

Table 1. BET surface area, electrode density and capacitance of prepared activated carbons.

Sample	BET surface area [m^2/g]	Electrode density [g/ml]	Capacitance		Ratio of capacitance in F/g (SK/SH)
			F/g	F/ml	
SK	2007	0.40	34.0	13.6	1.5
SH	1969	0.44	23.2	10.2	

Quantification, Electrolyte ion, Solid-state NMR

to ions adsorbed on free surface. On the other hand, broad peaks observed at higher magnetic field were considered to be due to ions adsorbed in pores. In the charged state, peaks were down-shifted, indicating de-shielding effect by attracting electrons of BF_4^- to the positive electrode. Furthermore, a peak at around -150 ppm was newly observed in the charged samples (marked with arrows).

In Table 2, sums of peak areas for all peaks in each spectrum are summarized. Here, the peak areas for BF_4^- were normalized by using those of PTFE main peak. A ratio of differences of the normalized BF_4^- peak areas between charged and discharged states for SK to SH was calculated to be 1.6, which was very close to the capacitance ratio of 1.5. That is, the quantitative analyses of the BF_4^- anions using the ^{19}F solid-state NMR showed a good correspondence to the capacities of KOH- and steam-activated carbons in EDLC system.

T_1 values of broad peaks are also shown in Fig. 1. For both SK and SH, T_1 became shorter upon charging, indicating strongly adsorbed states by electrostatic interactions between anions and the positively charged electrode. We also found that T_1 for SK was shorter than that for SH, suggesting the stronger interaction of ions in the pores of KOH-activated carbon than in those of steam-activated one. We considered that this is a reason why the KOH-activated carbon (SK) showed higher capacitance as compared with the steam-activated one (SH).

A 2D exchange spectrum is shown in Fig. 2. No correlation was found between two main peaks, but the newly appeared peak only in the charged state apparently correlated to a sharp peak originated as electrolyte anions adsorbed on free surface.

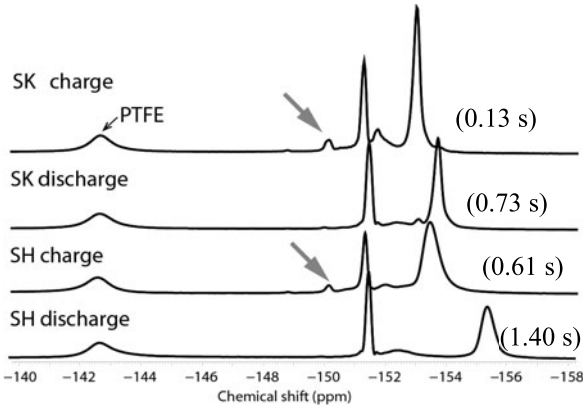

Fig. 1. ^{19}F NMR spectra of SK and SH at charged and discharged states. Numbers in parentheses indicate T_1 values of broad peaks.

Table 2. Normalized peak area of peaks in ^{19}F solid-state NMR spectra.

	Peak area of BF_4^-	Difference (ch-dis)	Ratio (SK/SH)
SK_{ch}	6.87	3.57	1.6
SK_{dis}	3.30		
SH_{ch}	6.46	2.17	
SH_{dis}	4.29		

※ Normalized BF_4^- by main peak of PTFE.

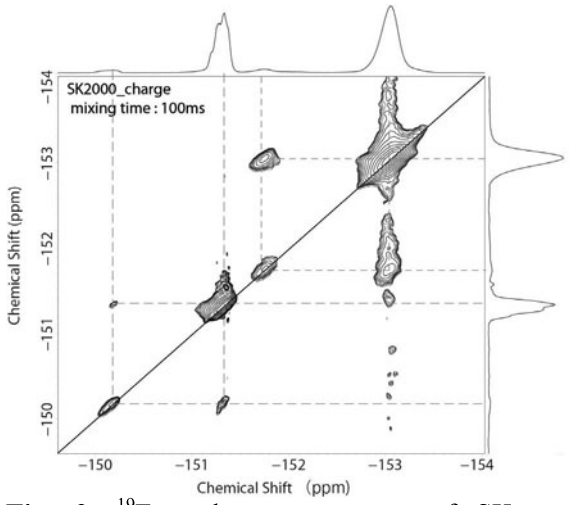

Fig. 2. ^{19}F exchange spectrum of SK at charged state.

4. Conclusion

The quantitative analyses of the BF_4^- anions using the ^{19}F solid-state NMR showed a good correspondence to the capacities of KOH- and steam-activated carbons in EDLC system. From the results of the relaxation time analyses, it was proved that the stronger interaction of ions in the pores of the KOH-activated carbon than that of steam-activated one, which could be a reason of higher capacitance of the KOH-activated carbon.

Acknowledgements

This work has done within the category of the Global-Centre of Excellence (G-COE) programs in Novel Carbon Resource Science, Kyushu University.

P-108 Evaluation of hydrogen gas dissolved in rubber material of O-ring for high-pressure Vessels

Hirotada Fujiwara[1], Junichiro Yamabe[1,2] and Shin Nishimura[1,3]
1) The Research Center for Hydrogen Industrial Use and Storage, AIST
2) International Research Center for Hydrogen Energy, Kyusyu University
3) Department Mechanical Engineering, Faculty of Engineering, Kyusyu University

[Abstract**]** Hydrogen dissolved in NBR after high-pressure hydrogen exposure has been analyzed using two methods of NMR and evaluated in terms of pressure dependency of free hydrogen to clarify the mechanism of fracture. Measurement using a sealed tube and solution state proves enabled the simultaneous analysis of dissolved hydrogen in rubber and hydrogen eliminated from the rubber. The result of ^{1}H MAS NMR suggested the two states of dissolved hydrogen. The difference of the relaxation time clarified the different mobility. Pressure dependency of the rate of the two kinds of hydrogen was also evaluated.

[Introduction**]** For the realization of society based on hydrogen as a next generational clean energy source, safety and reliability of materials for high- pressure hydrogen usage should be guaranteed. We have studied to establish a guideline of designing rubber materials for O-rings to join or seal high-pressure hydrogen storage vessels and conveyance pipes. We have reported rubber materials exposed to high-pressure hydrogen suffer blister fracture and swelling caused by dissolved hydrogen**.** [1,2)] In this study, to clarify the mechanism of the fracture, using solid state NMR, we characterized dissolved hydrogen in NBR after hydrogen gas exposure.

[Experiment**]** NBR without fillers such as carbon black: Acrylonitrile butadiene rubber (Nihon ZEON Nipol 1042) was employed as a material for specimen after sulfur and vulcanization accelerator were added. AVANCE-Ⅲ500MHz : Bulker Biospin was used for the measurement, and time dependency of spectra during hydrogen elimination was observed with single pulse sequence. The specimens filled in zirconia rotors were exposed to hydrogen in 100MPa and 20MPa at 30℃ for 24hours, and measured by solid MAS probe. A simultaneous analysis of gas eliminated from the specimens (4x4x60mm) was conducted by solution probe after they were sealed in ϕ10mm pressure resistant NMR tube. Chemical shift of free hydrogen gas was analyzed taking into account of the influence of temperature and pressure. A pressure resistant double tube with deuterium methanol was used to lock and measure temperature. Separately, hydrogen content was analyzed with TDA Thermal Desorption Analysis JSH-201: J-SCIENCE LAB CO., LTD.

[Results and discussion**]** ^{1}H spectra of specimen sealed in ϕ10mm tube exposed to 100MPa hydrogen using solution probe is shown in Fig.1 along with the ones of free hydrogen gas and crude rubber. A peak was detected around 7.3ppm as well as the broad peeks at 2.2ppm and 5ppm, which are derived from NBR main structure. [3)] The peak at 7.3ppm intensified with passage of time while the area at 4.6ppm attenuated. When the tube was unsealed the peak at 7.3ppm, [4)] which is equivalent to the chemical shift of free hydrogen gas measured separately, was disappeared. The conversion in the area of 4.6ppm and 7.2ppn suggests the change of dissolved hydrogen into free hydrogen eliminating from rubber.

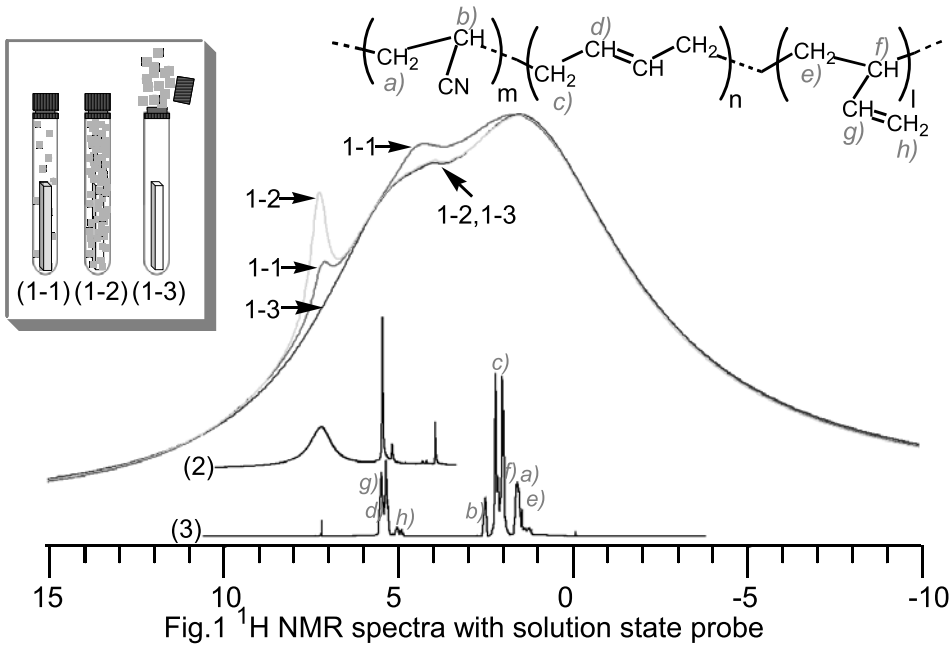

Fig.1 ^{1}H NMR spectra with solution state probe

(1)NBR during hydrogen elimination (30°C)with pressure resistant Φ10mm NMR tube. After exposure (-1) 5H sealed, (-2) 12.5H sealed, (-3) 12.5H unsealed.
(2) Free hydrogen gas / 0.6MPa (3) Solution state spectrum of crude rubber ($CDCl_3$)

Relationship between chemical shift of free hydrogen gas and pressure is shown in Fig. 2. Temperature of the free hydrogen gas, which affects the chemical shift, is ensured to be stable by chemical shift of Methanol. As a result Y(ppm)=-0.0669X(MPa)+7.2884 (Eq. 1) was derived. Here X is presser of hydrogen gas and Y is free hydrogen chemical shift.

The result of measurement for exposed specimens using solid-state MAS probe, is shown in Fig. 3 along with spectra of unexposed specimen. The spectra with MAS speed 3kHz shows two peak tops at 2.2ppm and 5.5ppm derived from NBR structure. On the other hand, in the spectra after exposure peaks were detected 4.5ppm[A] and 4.8ppm[B] as well. Spectra of high-resolution measurement with MAS speed 35kHz suggested that the peaks are not assigned to NBR structure. As the time passed, peak intensity attenuated to overlap the spectra of unexposed one. The hydrogen content in the specimen exposed to 100MPa was calculated from the rates of total area of A and B to the peaks derived from NBR. The change of the calculated hydrogen content in a period of time after hydrogen exposure is shown in Fig.4 along with the values simultaneously measured by TDA. It shows a good agreement of both values. [A] and [B] were suggested not to be derived from free hydrogen gas eliminated from specimen nor remained in rotors, because their chemical shift are different from free hydrogen

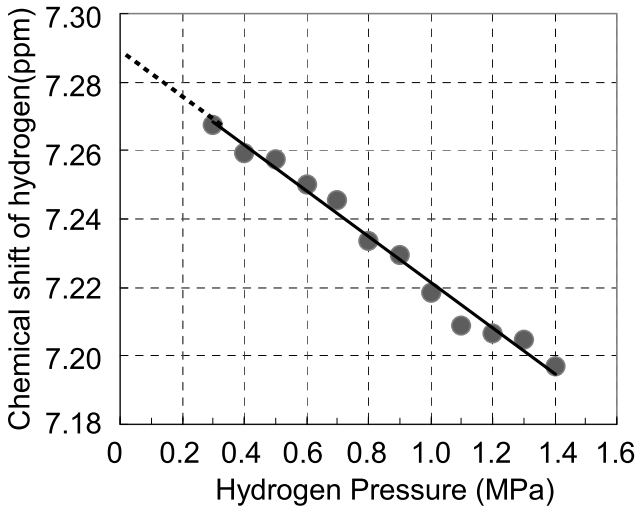

Fig.2 Influence of pressure on chemical shift (δ in TMS=0 ppm, 30°C)

gas of about 7.3ppm which we have already reported. The result shows that NMR can determine all hydrogen in rubber material. [4)]

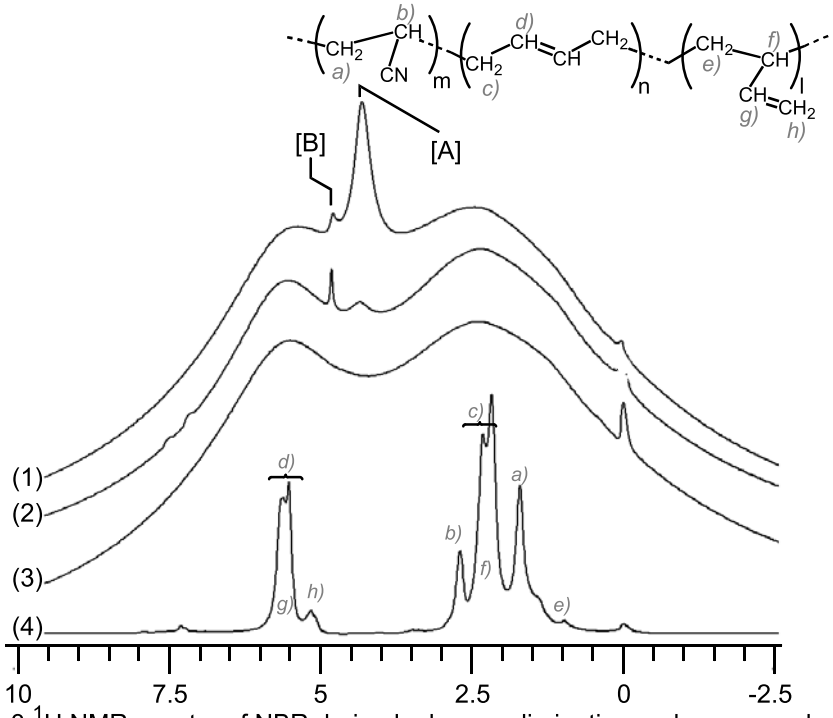

Fig.3 ^{1}H NMR spectra of NBR during hydrogen elimination and unexposed
(1) 1H after 100MPa exposure (MAS speed 3kHz)
(2) 1H after 20MPa exposure (MAS speed 3kHz)
(3) Unexposed (MAS speed 3kHz) (4) Unexposed (MAS speed 35kHz)

It is necessary to deny the possibility of [A] and [B] being free hydrogen gas of inner bubble in blister. Then the specimen exposed to 20MPa was analysed based on the idea that inner pressure in blister cannot be higher than exposure pressure. In the spectra after exposure, peaks [A] and [B] are detected as in 100MPa, and the chemical shift was not affected by exposure pressure. Chemical shift of free hydrogen gas exposed to 20MPa was calculated to be 5.95ppm with Eq. 1, which is different from [A] (4.5ppm) and [B] (4.8ppm). [A] and [B] are suggested not to be derived from free hydrogen in blister.

As a result, [A] and [B] are confirmed to be hydrogen dissolved in rubber. Relaxation time / T1 of [A] and [B] were determined to be 0.01s and 0.49s respectively and half width is greatly different each other. The rate of [A] to [B] increases according to the rise of exposure pressure. Then, it is suggested that

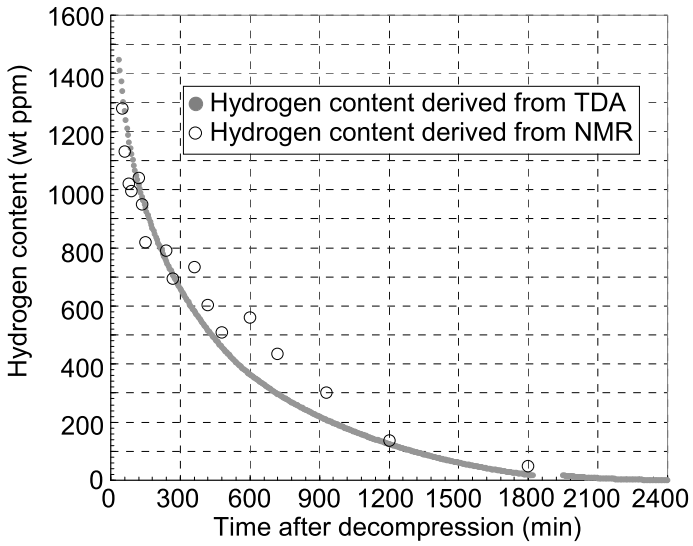

Fig.4 Isothermal profile of hydrogen content in elimination process measured by NMR and TDA (100MPa exposed spesimen)

hydrogen dissolved in rubber exists in two different states with greatly different mobility. The difference of the mobility is supposed to be caused by strength of interaction between hydrogen molecules and rubber molecules in crosslink structures.

1) J. Yamabe and S. Nishimura, Int. *J. Hydrogen Energy,* 34, 1977 (2009).
2) J. Yamabe, A. Koga and S. Nishimura, *Nippon Gomu Kyokaishi,* 83, 159 (2010).
3) H. Fujiwara, J. Yamabe and S. Nishimura, *KOBUNSHI RONBUNSHU* 66, 363 (2009)
4) H. Fujiwara, J. Yamabe and S. Nishimura, *Chemical Physics Letters*, 42, 498 (2010)

[Acknowledgement**]**
This research has been partly supported by the project ‘‘Fundamental Research Project on Advanced Hydrogen Science (2006–2012)” of New Energy and Industrial Technology Development Organization (NEDO), Japan.

Hydrogen gas, NBR (Acrylonitrile butadiene rubber), Rubber

P-110
Y

Investigation of Effects of Fluxing Agent Addition on Structural Transition of Coal Ashes by Solid-State NMR

Xiongchao Lin [1], Keiko Ideta [2], Jin Miyawaki [2], Isao Mochida [3] and Seong-Ho Yoon [1, 2]

[1] Interdisciplinary Graduate School of Engineering Sciences, Kyushu University, 6-1 Kasuga koen, Kasuga, Fukuoka 816-8580, Japan
[2] Institute for Materials Chemistry and Engineering, Kyushu University, 6-1 Kasuga koen, Kasuga, Fukuoka 816-8580, Japan
[3] Research and education center of carbon resource, Kyushu University, 6-1 Kasuga koen, Kasuga, Fukuoka 816-8580, Japan

ABSTRACT:

The effect of flux addition on the structural transition of coal ashes was investigated using ^{27}Al and ^{29}Si solid-state NMR. The effect of Ca ions that predominantly destroyed the octahedral Al and tetrahedral Al to pieces became remarkable with increasing its addition amount. On the other hand, Fe ions exhibited less effect on the framework structure than Ca ones. We also found that the flow properties of coal ashes were strongly affected by the Ca-flux addition because it brought about the segmentation of the Si-framework structure to less network one.

1. Introduction

To extend the utilization of high rank coals in coal gasification, more attention should be paid to solve the high viscosity of the ash, in which silica and alumina are primary components. In the present study, the transition behaviors of high viscosity coal ash were closely investigated by blending of $CaCO_3$ or iron oxides by using solid-state NMR.

2. Experimental

2.1 *Sample*

Datong coal from China with high SiO_2 and Al_2O_3 contents was used in this study.

2.2 *Methodologies*

The molten ashes were analyzed by means of 800MHz (for ^{1}H) solid-state NMR at a magnetic field of 18.8T. Viscosity was measured under N_2 atmosphere up to 1700^{o}C by a high temperature rotatory viscometer.

3. Results and discussion

3.1 Solid state NMR analyses

Fig. 1(I) shows the ^{29}Si solid-state NMR spectra of ash with 0, 10, 15, 20, 25 *wt.* % $CaCO_3$ addition, respectively. The sharp peak at -110.2 ppm was ascribed to the $Q^4(0Al)$,that is, quartz and/or amorphous silica. Peaks at -104.3 ppm, -99.5 ppm, -93.4 ppm and -86.0 ppm were attributed to $Q^4(1Al)$, $Q^4(2Al)$, $Q^4(3Al)$ and $Q^3(0Al)$, respectively[1, 2].

Solid state NMR, coal ash, fluxing agent

The 10 *wt.* % addition of $CaCO_3$ led to a slight broadening of peaks (Fig.1 (I) b). With increasing the addition ratio to 15 *wt.* %, the peaks shifted to downfield obviously; the fraction of Q^4(0Al) decreased apparently, while that of Q^2(1Al) at -84.3 ppm increased. These transitions indicate the destroying of large alumina-silicate framework structure by the added Ca ion to smaller size. The structural transformations became more obvious when the addition ratio up to 20, 25 *wt*. %, as shown in Fig.1 (I) d and e.

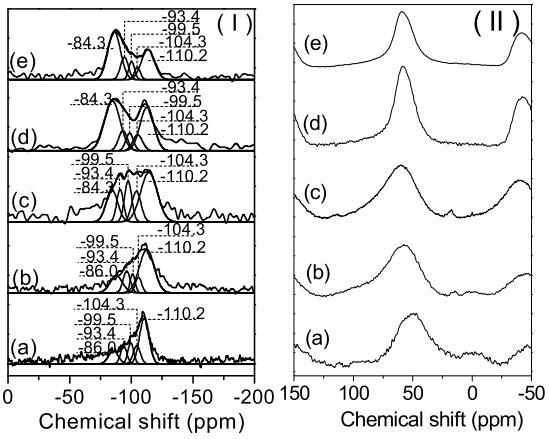

Fig.1. Solid state NMR spectra of Datong ash with $CaCO_3$ addition at different mixing amount after heat treatment at 1400°C. (I) ^{29}Si, (II) ^{27}Al.

All ashes after the heat treating at 1400°C were primary 4-coordinated Al, as shown in Fig. 1(II). Weak peak at around 4.7 ppm observed in raw Datong ash was due to poorly crystallized mullite that gradually disappeared with an increase of $CaCO_3$ addition up to 20-25 *wt*. %. The coordinative transitions of Al species with the fluxing agent addition implied the T-O-T structure being stable and predominant.

3.2 *Flow properties with fluxing agent addition*

The viscosities of ashes decrease with the CaO addition as shown in Fig.2. The *Tcv* (temperature of critical viscosity) of raw D ash at *ca.* 1580 °C decreases to *ca.* 1530 °C after 10 *wt.* % addition. The obvious change was occurred after the additional ratio increase to 15 *wt.* % that *Tcv* changed to *ca.* 1420 °C. The less Ca ions primarily play the charge balance in the framework (Fig.3a). The addition of $CaCO_3$ leads to the continuously decrease of viscosity due to the deeply loosen of polymeric structure (Fig.3b). Thus, the *Tcv* changes to *ca*. 1370 °C and 1320 °C after addition ratio up to 20 and 25 *wt* %, respectively.

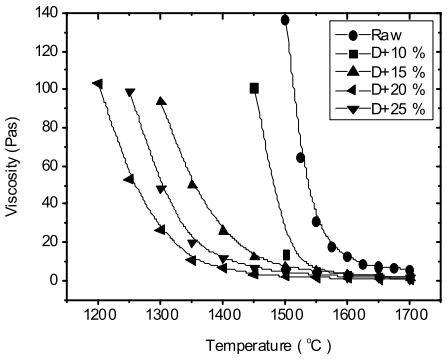

Fig.2. Viscosity tendencies of Datong ash with $CaCO_3$addition at different mixing amount.

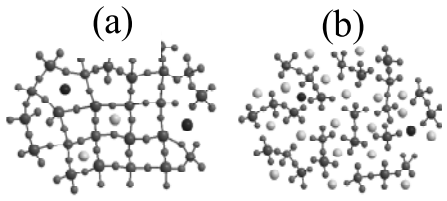

Fig.3. Molecular model of molten ash with $CaCO_3$ addition. (a) Small $CaCO_3$ addition amount, (b) Large $CaCO_3$ addition amount.

4. Conclusion

$CaCO_3$ addition effectively lessened the structural networks of Datong ash to fragments, giving rise to the decreases of macroscopic parameter of viscosity.

Acknowledgement

The authors are grateful to the supporting of NEDO, GCOE and Dr. Nishiyama from JEOL.

Reference

[1] Joao Rocha and Jacek Klinowski, *Phys Chem Miner* 17 (1990), p: 179-186.

[2] P. Pena, J.M. Rivas Mercury, A.H.de Aza, *J Solid State Chem* 181 (2008), p: 1744-1752.

P-111 Solid state NMR analysis of metal pyrophosphate composites as proton conductors

Masakazu Nishida[1], Tomoko Tanaka[1], Haruhiko Fukaya[1], Wataru Kanematsu[1] and Takashi Hibino[2]
[1]National Institute of Advanced Industrial Science and Technology
[2]Graduate School of Environmental Studies, Nagoya University

ABSTRACT

In order to investigate the proton conduction mechanism of various metal pyrophosphate composites (MP_2O_7-MO_2; M = Sn, Si, Ti, Zr) and the effect of the Sm doping on the proton conductivity, ^1H and ^{31}P MAS NMR analyses and relaxation time measurements were carried out between room temperature and 80 °C. Although some acidic protons were observed for the ^1H MAS NMR spectra of all the composites, their proton conductivity was closely correlated to the T_1H value rather than the intensity of the ^1H peak. For the ^{31}P MAS NMR spectra, the peaks of active species were found to disappear after water washing. Time- and temperature-depending changes of the spectra and the T_1H is also discussed.

INTRODUCTION

Because of relatively high proton conductivities in the temperature range of 200–600 ºC, metal pyrophosphates (MP_2O_7) are expected as promising electrolyte materials for solid oxide fuel cells, chemical sensors, and solid catalysts. Especially, of MP_2O_7, SnP_2O_7 has the highest proton conductivity (>10^{-2} S cm^{-1}), which is further improved by substituting a part of Sn^{4+} with low valence cations. For realizing practical applications, however, there are several technical subjects; for example, low mechanical strength of the pressed SnP_2O_7 pellet and poor stability of the pellet to the moisture. Against this background, we produced new MP_2O_7-based ceramics (M = Sn, Si, Ti, Zr), which were easily formed on the surface of a porous MO_2 substrate by reacting it with H_3PO_4.

MP_2O_7 has a cubic structure with MO_6 octahedra and P_2O_7 units at the corners and edges, respectively. We have previously studied ^1H and ^{31}P MAS NMR of SnP_2O_7 and acceptor-doped SnP_2O_7 to clarify the effect of such dopant cations on proton conductivity. In this study, we report the dynamics of protons in the MP_2O_7-MO_2 composite ceramics, in addition to the environment of the phosphate under various conditions by ^1H and ^{31}P MAS NMR analyses.

EXPERIMENTAL

The MP_2O_7–MO_2 composite ceramics were prepared by treating a porous MO_2 substrate with H_3PO_4 at 600 °C. The electrochemical properties of the MP_2O_7–MO_2 composite ceramics were investigated using two Au plates as electrodes. The NMR spectra were measured at ambient temperature with a Varian Unity Inova 300 NMR spectrometer in powder form. The recycled time was 10 sec for ^1H nuclei and 100 sec for ^{31}P nuclei, respectively. The spinning rate of the sample was set to 9 kHz. The values of T_1H and T_1P were calculated from the magnitudes of arrayed spectra obtained by the saturation recovery pulse sequence.

Proton conductivity, Counter cation effect, Dopant

RESULTS AND DISCUSSION

In Fig. 1, the conductivity of MP_2O_7-MO_2 composites ceramics were significantly affected by the M species (M: Sn > Si > Ti > Zr) and by doping (5 mol% Sm in SnP_2O_7-SnO_2).

To better understand the observed influences, first, we measured ^{1}H MAS NMR (Fig. 2), focusing on magnitudes and line shape of acidic protons. While the composite having the lowest conductivity, ZrP_2O_7, showed only a broad weak ^{1}H peak in free water region, the other composites had ^{1}H peaks in acidic proton region. The peak intensity of these acidic protons, especially in TiP_2O_7 and SiP_2O_7 composites, decreased with the time elapsed. The increase of ^{1}H peak intensity due to the moisture absorption was not observed, unlike the SnP_2O_7 powder.

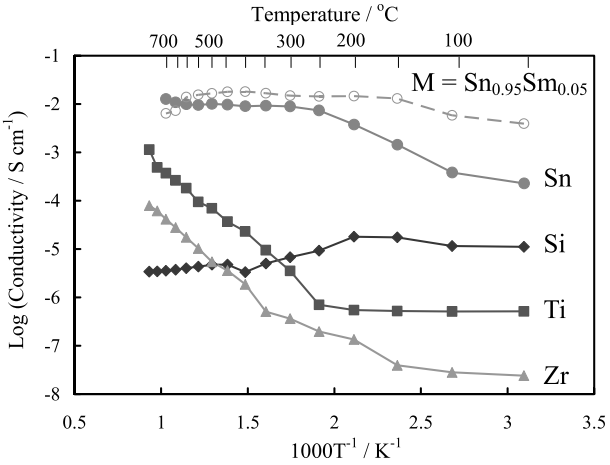

Fig.1 Conductivity of MP_2O_7-MO_2 composites (M = Sn, Si, Ti, $Sn_{0.95}Sm_{0.05}$)

Next, we examined phosphate species in the composite ceramics by ^{31}P DD-MAS NMR (Fig. 3). The TiP_2O_7 and SiP_2O_7 composites showed sharp ^{31}P peaks in the PO_4 region (*ca.* 0 ppm), indicating that these composites had excess amounts of H_3PO_4. However, since these phosphates are easily volatilized, it is likely that they do not contribute to the proton conductivity. The other composites ceramics did not show ^{31}P peaks in the PO_4 region, but had in the P_2O_7 region (30–50 ppm). These P_2O_7 peaks are assigned to the bulk phosphates, which were little affected by H_2O. Several sharp ^{31}P peaks in relative lower P_2O_7 area (dotted circle), which could be removed by water washing, are considered to be active species that are concerned with the proton conductivity.

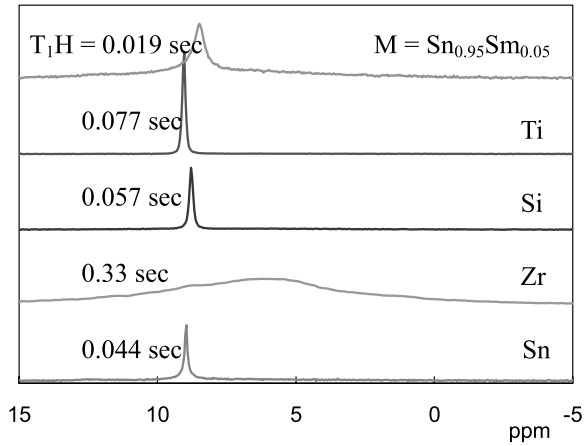

Fig.2 ^{1}H MAS NMR and T_1H of MP_2O_7-MO_2 composites (M = Sn, Si, Ti, $Sn_{0.95}Sm_{0.05}$)

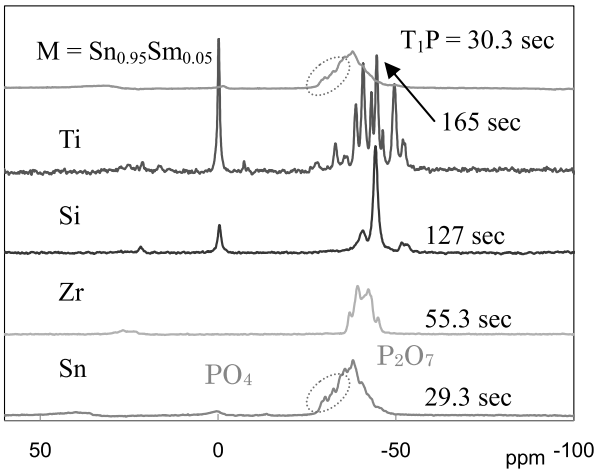

Fig.3 ^{31}P MAS NMR and T_1P of MP_2O_7-MO_2 composites (M = Sn, Si, Ti, $Sn_{0.95}Sm_{0.05}$)

Based on the above observations, there are three possible kinds of phosphates in different environments: *a*) the bulk P_2O_7, *b*) the surface P_2O_7, *c*) excess free H_3PO_4. The proton conductivity would be caused by a proton hopping through the type *b* of P_2O_7, which leads to the short T_1H value (in Fig. 2). It is also possible that excess H_3PO_4 (type *c*) prevented the proton hopping to decrease the conductivity as well as to increase T_1H and T_1P values. We are now examining changes of spectra and T_1 value under various conditions in more details.

P-112 Solid-state NMR study of the local arrangement of C_{60} molecules in C_{60}-graphite nanocomposite

Daisuke Kuwahara[1], Daisuke Inoue[1], Masaru Suzuki[1],
Toshikazu Nakamura[2], Makoto Ishikawa[3] and Koji Miura[3]

[1]The University of Electro-Communications
[2]Institute for Molecular Science
[3]Aichi University of Education

Abstract

We present a new version of the REDOR techniques for a homonuclear spin pair undergoing magic angle spinning (MAS). Using this version, the variation of the MAS line intensities is caused by the dipolar coupling between a homonuclear spin pair in solids. In this study, this new version was applied to a C_{60}-graphite nanocomposite under MAS. For this composite, C_{60} is uniformly ^{13}C labeled, while the graphite sheets have natural abundance ^{13}C's. As a result, the reduction of the rotational echo of the C_{60} ^{13}C resonance was observed. This experimental result elucidated that the C_{60} molecules were intercalated between the graphite sheets in the nanocomposite.

Introduction

Today, measurement of heteronulcaer dipolar couplings on biomolecular samples undergoing MAS are often made in the solid-state NMR applications. For such NMR experiments, one of the most widely used methods is rotational-echo double-resonance (REDOR). In this study, we present a new version of the REDOR techniques for a homonuclear spin pair undergoing MAS.

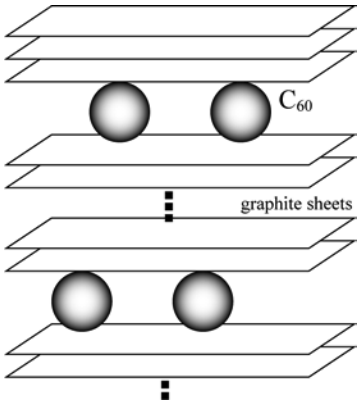

Figure 1. Schematic representation of the C_{60}-Gs nanocomposite.

The REDOR techniques have thus far been used to accurately determine internuclear distances of interest in solids. In this study, we employ the new version in order to elucidate whether or not C_{60} molecules are located between the graphite sheets in a C_{60}-graphite nanocomposite (C_{60}-Gs) [1].

C_{60} in C_{60}-Gs yields a sharp resonance line under MAS conditions. On the other hand, the graphite sheets in C_{60}-Gs yield a very broad resonance line with a line width of several hundred ppm under the condition of a low spinning speed. Thus, the nanocomposite can be said to have a markedly different character from a variety of chemical systems, to which the REDOR techniques have often been applied so far. We demonstrate that the new version of REDOR techniques can contribute also to researches in the field of material science such as the research on the local structure of the C_{60}-Gs nanocomposite.

C_{60}, graphite, REDOR

Theory

The pulse sequence employed in this study is presented in Fig. 2. This pulse sequence is applied to a pair of homonuclear nuclei with spin angular momenta, *S* and *I*. In order to quantitatively confirm that the REDOR phenomenon occurs at $t = 2T_r$ on the pulse sequence of Fig. 2, we calculated the analytical expression of the average Hamiltonian for the pulse sequence. As a result, we obtained the following significant information: when the ratio of the chemical-shift difference of the homonuclear spin pair to the spinning speed is greater than 9, the average Hamiltonian becomes equivalent to that of a heteronuclear spin pair (ex. $^{13}C-^{15}N$). The average Hamiltonian under the above condition is given by

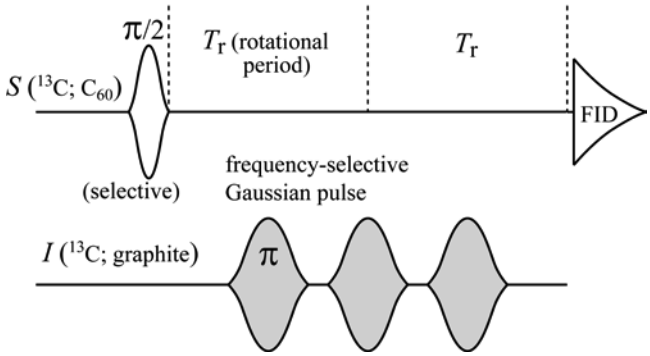

Figure 2. Pulse sequence employed in this study.

$$\overline{\mathcal{H}_d^{(0)}} = -\frac{1}{\pi}\tilde{a}_s^{(1)} d_{12}^{(1)}(\beta)\sin\gamma\cdot(2I_z S_z) - \frac{1}{\pi}\sum_{m=1,2}\tilde{a}_c^{(m)} d_{12}^{(m)}(\beta)\cos m\gamma\cdot(2I_y S_z)$$, where $\tilde{a}_s^{(1)} = 3.912$, $\tilde{a}_c^{(1)} = -1.113$, and $\tilde{a}_c^{(2)} = 0.318$.

Results and Discussion

Figure 3 shows the experimental results of the REDOR experiments performed on the C_{60}-Gs nanocomposite spinning at 1kHz. Both spectra in Fig. 3 were measured using the pulse sequence of Fig. 2. The spectrum depicted with a solid line was obtained using the following irradiation frequencies: ω_S = 144ppm (the resonance line of C_{60}) and ω_I =10ppm, where ω_S and ω_I are, respectively, the irradiation frequencies for the two spins, *S* and *I*. Note that 10ppm is within the spectral distribution of the resonance line for the graphite sheets. On the other hand, the spectrum depicted with a broken line was obtained under the condition of $\omega_S = 144$ppm and ω_I =278ppm, which is out of the spectral distribution for the graphite sheets. It should be noted that we tried to detect the REDOR phenomena between the single C_{60} resonance and the graphite sheet resonances contained in a segment (around 10ppm) in the wide resonance line. We can clearly see the reduction of the rotational echo on the spectra in Fig. 3, and the reduction is ca. 5% of the full echo intensity. This experimental result suggests that the C_{60} molecules are located adjacent to the graphite sheets. When the experimental results of powder X-ray diffraction of the C_{60}-GS nanocomposite [1] is considered together, we may say that the C_{60} molecules are intercalated between the graphite sheets as expected.

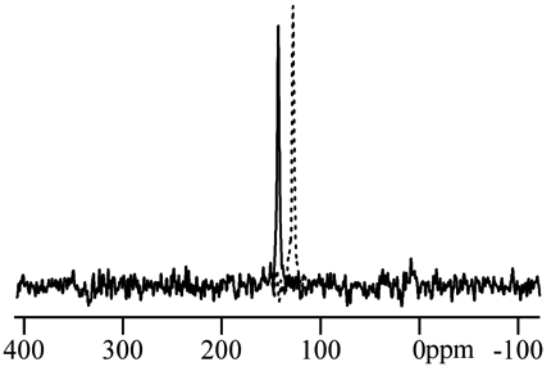

Figure 3. NMR spectra for C_{60}-Gs nanocomposite. These spectra were measured using the pulse sequence of Fig. 2.

[1] N. Sasaki and K. Miura, Jpn. J. Appl. Phys. **43**, 4486 (2004).

P-113 Solid-state ^{19}F NMR study on the chemical state of trace amounts of fluorine in $CaO\text{-}SiO_2$ and $CaO\text{-}Al_2O_3\text{-}SiO_2$ systems

Takafumi Takahashi and Koji Kanehashi
Advanced Technology Research Laboratories, Nippon Steel Corporation

ABSTRACT
The chemical state of trace amounts of fluorine (F≤ 2.0*mass*%) in slowly cooled $CaO\text{-}SiO_2$ and slowly-/rapidly-cooled $CaO\text{-}SiO_2\text{-}Al_2O_3$ systems has been investigated by solid-state ^{19}F NMR. A new F-less NMR probe enables us to acquire good quality ^{19}F-MAS NMR spectra of the trace F without background suppression using depth pulse train. ^{19}F-MAS spectra for the $CaO\text{-}SiO_2$ systems demonstrate that F occurs as cuspidine ($Ca_3Si_2O_7F$) and fluorite (CaF_2) in CaO/SiO_2 (C/S) ratio of 1.0-2.0, while F in the lower C/S ratio (=0.5) is incorporated into the amorphous phase. For the slowly-cooled $CaO\text{-}SiO_2\text{-}Al_2O_3$ system with the constant 50*mass*% Al_2O_3, the effect of aluminum (Al) on F chemical states changes depending on the C/S ratios; the Al-F bonding is suggested in the low C/S region of 0.5, while the Ca-F bonding is formed in the higher C/S ratios (1.0-2.0). The $^{19}F\{^{27}Al\}$ TRAPDOR spectra of rapidly-cooled samples indicate that a certain amount of Al-F bonding is formed at a wide range of C/S ratios, which suggests that F and Al ions are at close range in the corresponding melt systems.

Introduction

In both geological and industrial field, F anions partially substituting for oxygen in silicate and aluminosilicate melts are known to drastically change physical properties and phase equilibria. These characteristics are mainly due to its strong electronegativity. In steel-making processes, F is utilized to control viscosity, crystallization behaviour, and solidification temperature of mold flux. Furthermore, the F-glasses are well-known promising materials for the optical applications, because of their wide range of optical transmittance and low phonon energy. The ^{19}F-solid state NMR studies applied to the analysis of F chemical environments in silicates have treated with relatively high content of F (>7 *mass*%) and not suffered from the obstruction of F background signals. In the present study, to extend the possibility of ^{19}F NMR analysis to materials with lower F concentrations, we have studied the chemical state of trace amounts of F (≤ 2*mass*%) in $CaO\text{-}SiO_2$ and $CaO\text{-}Al_2O_3\text{-}SiO_2$ systems, and the cooling-rate effects on F chemical environments in $CaO\text{-}Al_2O_3\text{-}SiO_2$ systems by ^{19}F MAS and $^{19}F\{^{27}Al\}$ transfer of population in double resonance (TRAPDOR) NMR[1] with a new F-less NMR probe.

Experimental

Sample preparation

Samples designed to have the compositions shown in Table 1 are synthesized from regent grade $CaCO_3$, SiO_2, Al_2O_3, and CaF_2. The mixtures of $CaCO_3$, SiO_2, and Al_2O_3 in a platinum (Pt) tube

^{19}F, TRAPDOR, glass

were preheated at 900°C in an electric furnace for decarbonation, and then small amounts of CaF_2 were added. The Pt tube tightly sealed to avoid the vaporization of F were heated to 1680°C and kept for one hour. Some vessels were slowly cooled (8°C/min) in an electronic furnace for preparation of crystalline samples, and the others were rapidly cooled (500°C/min) for preparation of glasses.

Table 1. Chemical composition of prepared samples.

Sample no.	CaO(mass%)	SiO_2(mass%)	Al_2O_3(mass%)	F(mass%)	CaO/SiO_2	Cooling rate
CS0.5-S	33	66	-	1	0.5	Slow
CS1.0-S	49.5	49.5	-	1	1	Slow
CS2.0-S	66	33	-	1	2	Slow
CS0.5-A-S	16	33	50	1	0.5	Slow
CS1.0-A-S	25	25	50	1	1	Slow
CS2.0-A-S	33	16	50	1	2	Slow
CS0.5-A-S	16	32	50	2	0.5	Rapid
CS1.0-A-S	24	24	50	2	1	Rapid
CS2.0-A-S	32	16	50	2	2	Rapid

NMR experiments

All NMR experiments were performed on a JEOL ECA-700 spectrometer equipped to a 16.4*T* narrow bore magnet using a $^{19}F\{^{27}Al\}$ double resonance probe with 3.2 mmϕ ZrO_2 rotors. The F background derived from a probe was suppressed by adopting F-free materials for probe assemblies. The ^{19}F-MAS NMR spectra were acquired using 18° pulse (0.7 μs), spinning frequency of 20 kHz, and recycle delay of 3s. In TRAPDOR experiments, the rotor-synchronized 90°-180° pulse sequence as shown in Fig.1 was applied to the ^{19}F nuclei with the recycle delay of 60s, while irradiation pulses were applied to ^{27}Al nuclei with the RF strength of 13.5 kHz during both the evolution and the refocusing periods. The TRAPDOR fraction demonstrates the reduction of its signal intensity with respect to that obtained without irradiation.

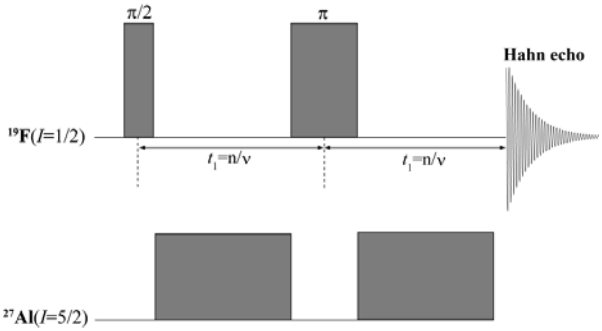

Fig. 1. $^{19}F\{^{27}Al\}$ TRAPDOR pulse sequence. The time t_1 is rotor-synchronized (with $1/\nu$ being the rotor period). No irradiation pulse is applied for ^{27}Al to record the reference spectrum.

Results and Discussion

The ^{19}F-MAS NMR spectra for CaO-SiO_2 and CaO-Al_2O_3-SiO_2 systems are shown in Fig.2. In slowly cooled CaO-SiO_2 system with the C/S ratio of 1.0-2.0, F occurs as cuspidine ($Ca_3Si_2O_7F$) (-99, -103 ppm) and fluorite (CaF_2) (-108 ppm), while in the lower C/S ratio of 0.5, F is incorporated into the amorphous phase. When compared with those of the same C/S ratio, the ^{19}F

NMR spectra for $CaO\text{-}SiO_2\text{-}Al_2O_3$ systems are obviously changed. In the high C/S composition (1.0-2.0), cuspidine is no longer observed, although the region of ^{19}F chemical shift (-100 to -110 ppm) still corresponds to the Ca-F bonding. With the decrease of C/S ratio (0.5), the NMR peak is shifted to upper field (-150 ppm), which suggests the Al-F bonding. In the ^{19}F-MAS NMR spectra of glass (rapidly-cooled) samples, the broad resonance considered to be Al-F bonding is observed at almost the same position, suggesting that a certain degree of Al-F bonding exists in the molten state even in high C/S regions.

$^{19}F\{^{27}Al\}$ TRAPDOR experiments were performed to confirm the existence of Al-F bonding,. A $^{19}F\{^{27}Al\}$ TRAPDOR spectrum is obtained as a difference between two spectra recorded with and without irradiation for ^{27}Al. A loss of echo intensity in a dephase spectrum is generated, compared with reference one, when ^{19}F nuclei are close to ^{27}Al nuclei in proximity due to the recoupling of dipolar interaction. As a consequence, resonances affected by strong dipolar couplings between ^{19}F and ^{27}Al nuclei (ex. Al-F bonding) are observed in a $^{19}F\{^{27}Al\}$ TRAPDOR spectrum. As shown in Fig. 3, the broad resonance is observed at approximately -150 ppm in $^{19}F\{^{27}Al\}$TRAPDOR spectrum of a slowly cooled sample with C/S ratio of 0.5 in the $CaO\text{-}SiO_2\text{-}Al_2O_3$ system. For a rapidly-cooled sample, two broad resonances are observed in the $^{19}F\{^{27}Al\}$ TRAPDOR spectrum. The resonance in the upper field (-150 ppm) is assigned to Al-F direct bonding as well as in the slowly cooled sample. However, it is not adequate to assign the resonance observed in a down filed (-100 ppm) to Al-F bonding, because it corresponds to the chemical shift region of Ca-F bonding[2]. This phenomenon is considered to be caused by through-space dipolar coupling between Al nuclei and F nuclei which belong to Ca-F bonding.

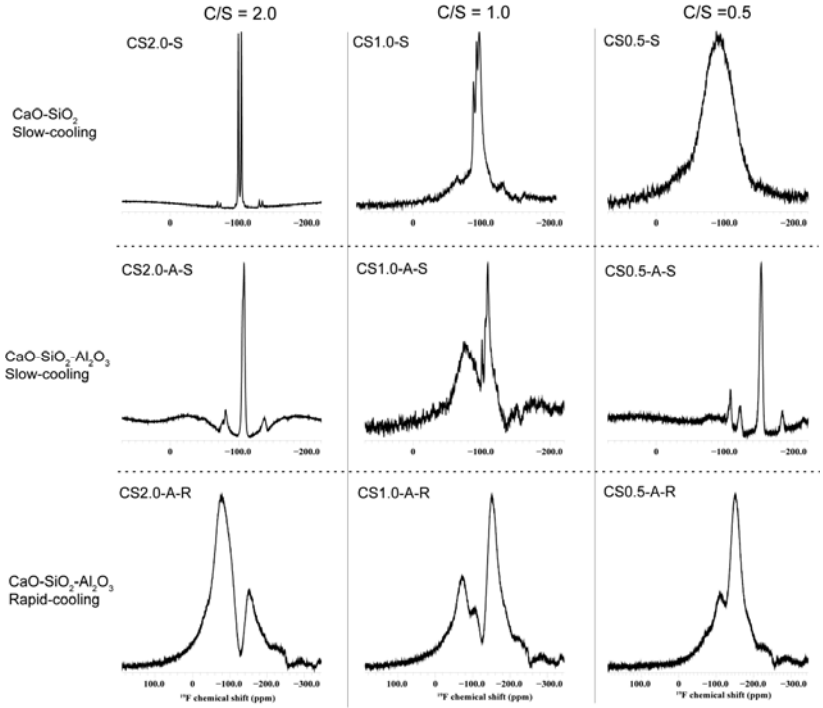

Fig. 2. ^{19}F-MAS NMR spectra of synthesized $CaO\text{-}SiO_2$ and $CaO\text{-}SiO_2\text{-}Al_2O_3$ samples with trace amounts of F. In the row direction, the spectra are categorized according to the whole composition and the cooling rate. In the column direction, they are categorized according to the CaO/SiO_2 ratios.

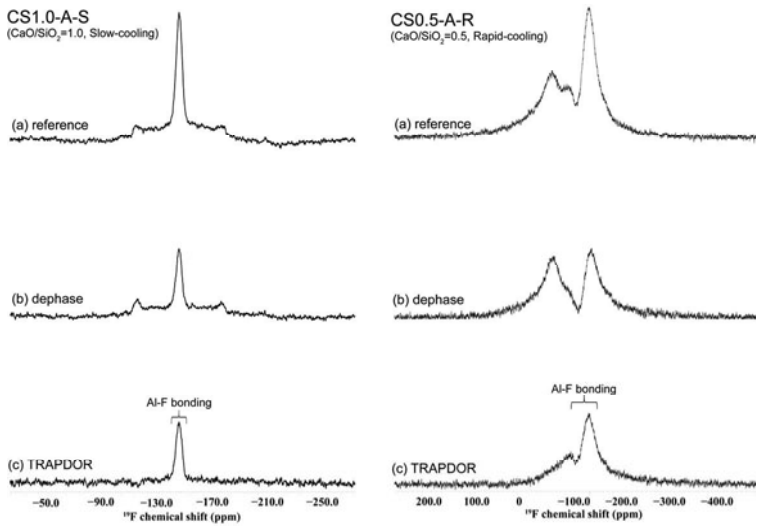

Fig. 3. $^{19}F\{^{27}Al\}$ TRAPDOR spectra for $CaO\text{-}SiO_2\text{-}Al_2O_3$ samples. All spectra were acquired at dephasing time of $2t_1$= 0.996ms. (a) Reference spectra obtained without irradiation for ^{27}Al. (b) Dephase spectra obtained with irradiation for ^{27}Al. (c) TRAPDOR spectra obtained as a difference of (a) and (b).

Since the $^{19}F\{^{27}Al\}$ TRAPDOR spectra of the other glass samples also show resonances at around -150 ppm, there is a certain amount of Al-F bonding for various CaO/SiO_2 ratios although the proportion of Al-F bonding increases in a lower CaO/SiO_2 system. Such a characteristic as well as that in the series of ^{19}F MAS spectra of slowly cooled $CaO\text{-}SiO_2\text{-}Al_2O_3$ systems indicates that the relative proportion of Ca^{2+} ions has significant influence on the F^- chemical state; the number of F^- ions bonded with Ca^{2+} ions becomes smaller as the C/S ratio declines. It is considered that Al^{3+} ions can be easily close to F^- ions in proximity and directly make bonds with F^- when the number of Ca^{2+} ions which prefer to make bonds with F^- ions decreases, suggesting that the aluminosilicate structure in molten state fairly changes depending on the C/S ratio. In contrast to slow-cooing systems, F^- ions exposed to rapid cooling have no time enough to diffuse sufficiently, and consequently preserve information in the molten state. The ^{19}F resonances affected by F-Al dipolar coupling in glasses, therefore, suggest that F^- ions are originally in close proximity to Al^{3+} ions in melts. Based on the results, the cooling rate is an important factor to control F chemical states in the solidified $CaO\text{-}SiO_2\text{-}Al_2O_3$ system.

Conclusions

- ✓ The fluorine chemical state in $CaO\text{-}SiO_2$ systems changes depending on the C/S ratios. Also in the $CaO\text{-}SiO_2\text{-}Al_2O_3$ systems, the effects of Al on F chemical states are observed depending on the C/S ratios; in the low CaO composition (C/S=0.5), the F^- ions directly bond with Al^{3+} ions, while at the higher CaO composition (C/S > 0.5), F^- ions prefer to make bonds with Ca^{2+} ions.
- ✓ The cooling rate is also an important factor to control F chemical states in the solidified $CaO\text{-}SiO_2\text{-}Al_2O_3$ system. The $^{19}F\{^{27}Al\}$ TRAPDOR spectra demonstrates that the Al-F bonding is formed in rapidly cooled samples. This result suggests that F^- ions and Al^{3+} ions occur at close range in the corresponding melts. This situation is contrast to that in the slow-cooled system, where F^- ions can diffuse sufficiently and F-bearing phases deposit according to phase equilibria.

References

1. A. Goldbourt, S. Vega, *J. Magn. Reson.* **154** (2002) 280-286
2. T.J. Kiczenski and J.F. Stebbins *J. Non. Crys. Solids* **306** (2002) 160-168

P-114 Application of very fast magic angle spinning module in the solid state with a sample tube diameter of 1mm to characterization of mass-limited materials

Yu Suzuki[1], Koji Yazawa[1], Yuko Miwa[2], Tadashi Shimizu[3], Katsuya Hioka[4], Yusuke Nishiyama[4], Atsushi Asano[5], Yoshitaka Ishii[6] and Tetsuo Asakura[1]

[1]Tokyo University of Agriculture and Technology (Japan)
[2]Toray Research center (Japan)
[3]National Institute for Materials Science (Japan)
[4]JEOL RESONANCE (Japan)
[5]National Defense Academy (Japan)
[6]University of Illinois at Chicago (USA)

ABSTRACT

The very fast magic angle spinning module in the solid state with 1mm outer diameter sample tube was developed. We reported some applications of this module to characterization of mass-limited materials. 1. Determination of inter-molecular structure of peptides using ^{1}H NMR spectra. 2. Atomic-level conformational analysis of ^{13}C labeled β-amyloid peptide using ^{13}C-^{13}C 2D NMR. 3. Deterioration analysis of LED encapsulation resin using ^{1}H NMR.

INTRODUCTION

As one of the methods to improve the low NMR sensitivity, we have developed micro-coil MAS NMR for mass-limited samples. In this work, the very fast magic angle spinning module (70KHz) in the solid state (1mm outer diameter sample tube) is newly developed. We will report some applications of this module to characterization of several mass-limited materials.

RESULTS AND DISCUSSION

1. High-resolution solid state ^{1}H NMR spectra of peptides.

Determination of inter - molecular arrangement of peptides is highly expected with solid state ^{1}H NMR. For example, CRAMPS NMR has been used for obtaining high-resolution ^{1}H NMR spectra, but this method was confronted with difficulty in quantitative analysis. Instead of this, well-resolved solid state ^{1}H NMR spectra have been successfully recorded by very fast MAS experiment.

Here, we attempt to record very fast ^{1}H MAS spectra of crystalline alanine tripeptide $(Ala)_3$ with anti-parallel (AP) and parallel (P) structures using very fast magic angle spinning module (70KHz) with 1mm outer diameter sample tube. As shown in Figure 1, well-resolved ^{1}H NMR spectra were available for each proton owing to the better spectral resolution achieved by 70kHz MAS spinning. The difference in the inter-molecular

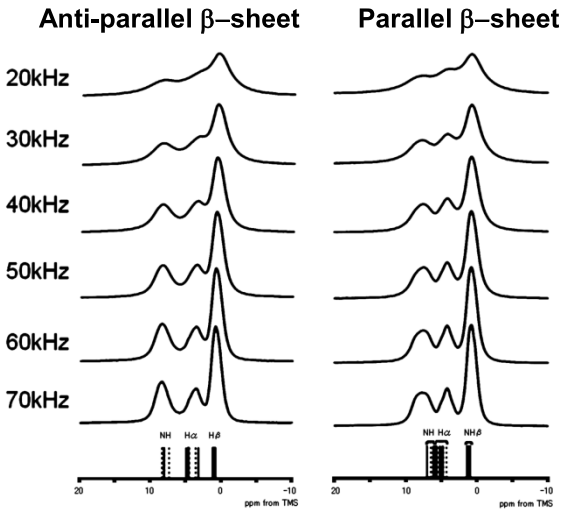

Figure 1 ^{1}H NMR spectra of anti-parallel and parallel $(Ala)_3$ with 20~70kHz MAS rates and the stick spectra obtained by semi- empirical chemical shift calculation (bottom).

arrangement between AP and P could be examined from these spectra. Especially, the observed ^{1}H hydrogen bond shifts of the amide protons turned out to be very convenient probes to distinguish the AP and P β-sheet forms by examination of the hydrogen-bonding patterns together with the semi-empirical chemical shift calculation.

2. Structural analysis of β-amyloid with very fast MAS and low power ^{1}H RF decoupling.

Amyloid β-peptide(Aβ) is a major component of plaques in Alzheimer's disease, and the aggregate of Aβ has been shown high neural toxicity. This aggregate is insoluble and forms disordered structure, therefore solid state NMR is the most promising method to determine the structure.

The ^{13}C-^{13}C 2D NMR spectrum with only 1mg of Cu^{2+}-Aβ complex was successfully recorded by fast MAS (20kHz) at high magnetic field (800MHz) only in 4.2 hours as shown in Figure 2(a). However, hydrated proteins denature easily by heat. So it is crucial to avoid the heating due to very fast rotor spinning and high RF pulse. To suppress the heating due to ^{1}H RF decoupling which is necessary for high-resolution solid state NMR, low power ^{1}H RF decoupling was tested for L-isoleucine. The resolution of L-isoleucine spectra obtained under 70kHz MAS rate and 10kHz ^{1}H RF decoupling is as well or better than that obtained under 19kHz MAS rate and 100kHz ^{1}H RF decoupling shown in Figure 2(c,d). As the amount of heat is produced in proportion to RF power, the heat could be suppressed to about 1/100 under very fast MAS and low power ^{1}H RF decoupling.

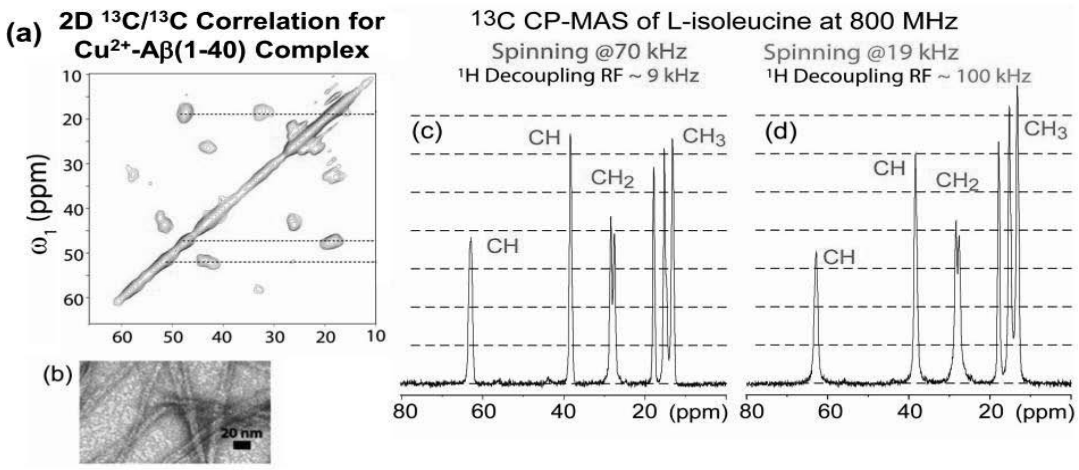

Figure 2 (a) Solid state ^{13}C-^{13}C 2D NMR spectrum of Aβ. (b) electron microscope image Aβ fibril. (c,d) The ^{13}C-CPMAS spectra of L-leucine under 70kHz MAS and ~9kHz ^{1}H RF decoupling (c) and 19kHz MAS and ~100kHz ^{1}H RF decoupling (d).

3. Deterioration analysis of LED encapsulation resin

Very small amount of LED encapsulation resin was analyzed using this method. Under overvoltage condition, small increase of cross-linked structure was detected and the major structural changes were not observed. This study shows that NMR analysis in high sensitivity could be achieved for mass-limited materials by using microprobe NMR.

ACKNOWLEDGEMENT

The authors acknowledge the financial support from SENTAN, JST and from Grant-in-Aid for Scientific Research from Ministry of Education, Science, Culture and Supports of Japan (23245045) and (21550112).

Keyword: solid state NMR, micro probe NMR, fast magic angle spinning

P-115
Y

Ex-situ ^{7}Li MAS NMR of a lithium cobalt oxide thin film on sequential annealing

Yasuto Noda[1], Munehiro Inukai[2] and Kazuyuki Takeda[1]
[1]Division of Chemistry, Graduate School of Science, Kyoto University
[2]Institute for Integrated Cell-Material Sciences, Kyoto University

We have developed a novel approach to non-destructive MAS NMR for thin-film samples, and successfully traced the sequential annealing effects on the local structure of a 200 nm-thick $LiCoO_2$ film by ex-situ ^{7}Li MAS NMR. The results suggest that in the first annealing period of 3 minutes, the film transformed from the amorphous to crystalline phase. Further, we found that many oxygen defects remained even after 6th annealing period of 18 minutes.

Introduction

Thin-film lithium-ion batteries (TFLIBs) are composed of solid films of anode, solid electrolyte, and cathode materials deposited on a substrate. TFLIBs are highly safe, light, and flexible batteries, while retaining the favorable properties of lithium ion batteries, such as high-energy density and long lifetime.[1] For cathode materials of TFLIBs, $LiCoO_2$ is widely adopted out of various candidates. The $LiCoO_2$ thin films are prepared by physical vacuum vapour processes, followed by annealing treatment for increasing crystallinity. Their characterization is of interest because the lifetime and the capacity of TFLIBs strongly depend on the state of the cathode.

Solid-state NMR (SSNMR) is a powerful tool to extract information of the local and electronic structure in the cathode materials of lithium ion batteries.[2] SSNMR enables analysis of highly disordered systems, and can complement characterization by the other methods. However, it has not been widely used in the studies of the thin-film devices.

One of the reasons is that the conventional high-resolution SSNMR employs a cylindrical container optimised for magic angle spinning (MAS),[3, 4] which is an essential technique providing high-resolution spectra of polycrystalline samples by mechanical sample rotation around an axis tilted at the magic angle (54.7°) to the external magnetic field. A few MAS NMR works on the thin-film samples reported so far resorted to either scratching the sample off the substrate before being packed into the rotor[5-9], or stacking many small pieces of the films that fit in the rotor[10-12]. These approaches require tedious sample preparation. Furthermore, the experiments destroy the sample, hampering ex-situ characterization of the thin film devices. So far, nondestructive SSNMR analyses of the thin films have only been feasible in non-spinning samples,[13] in which high-resolution measurement is limited to samples without anisotropic structure.

For non-destructive analyses of thin films using high resolution SSNMR, we have developed a novel MAS method, named as disk MAS.[14]

Non-destructive MAS NMR for thin-films: disk MAS

Fig. 1(a) schematically depicts the method. A disk-shaped sample is put on the top of a rotor via an attachment, and spun together with the rotor at the magic angle by a conventional spinning module. This is an analogue of microcoil-MAS with a capillary tube put on the top of a rotor,[15-17]

Keywords: thin films, solid state NMR, ex-situ

however, spinning of a flat body requires more careful adjustment of the weight balance, as the moment of inertia for the disk is much larger than that for the capillary. Using a jig, we glued a circular quartz substrate to an attachment at the exact coaxial position, which was then mounted on the top of a Varian 4 mm rotor. We verified stable spinning at 7 and 14.2 kHz for sample diameters of 12 and 7 mm, respectively, whereas the nominal maximum spinning speed for the unmodified system was 15.0 kHz. Furthermore, we found that even a square quartz substrate with a length of 8 mm was stably spun at 7 kHz, by positioning its center of mass on the spinning axis precisely.

In order to apply radio frequency (r.f.) pulses to the thin-film sample and detect NMR signals, an additional probe, named a disk MAS probe, is fixed on the spinning module, as described in Fig. 1(a). The main body of the disk MAS probe is a compact board, on which a coil and capacitors are placed. The coil was wound with a silver wire. Its diameter, length, and number of turns were 14 mm, 5 mm, and 3, respectively. The circuit was tuned at 116.4 MHz, which corresponds to the ^{7}Li Larmor frequency in a magnetic field of 7 T. The quality factor was measured to be 150.

To calibrate the r.f. amplitude and r.f. inhomogeneity, we carried out ^{7}Li nutation experiments with 1 M LiCl aqueous solution. The liquid sample put in a cylindrical container with a diameter of 12 mm and a depth of 400 μm was placed at the position where the disk sample was to be located. The container was made of a Teflon rod. Using a lathe, a pit with a depth of 400 μm was made on the rod, from which a disk-shaped container was cut. Then, the pit was sealed with a cover glass, and the liquid reference sample was injected. KBr powder was packed into the rotor, so as to adjust the magic angle through measurement of the rotational echoes of the ^{79}Br FID using the coil of the MAS probe. Even though the thin film was axially off the magnet center, magnetic field homogeneity of less than 1 ppm was attained by the conventional shimming.

Fig. 1(b) shows power dependence of the r.f. amplitude for the disk MAS probe. For comparison, the result obtained using a home-built 4 mm MAS probe, whose quality factor was measured to be 41, is also plotted. We verified that the r.f. efficiency of the disk MAS probe was lower than that of the MAS probe only by a factor of 2.0. This is ascribed to the higher quality factor of the disk MAS probe (150). From the decay of the nutation curve, the r.f. inhomogeneity was estimated to be ca. 16% over the sample volume.

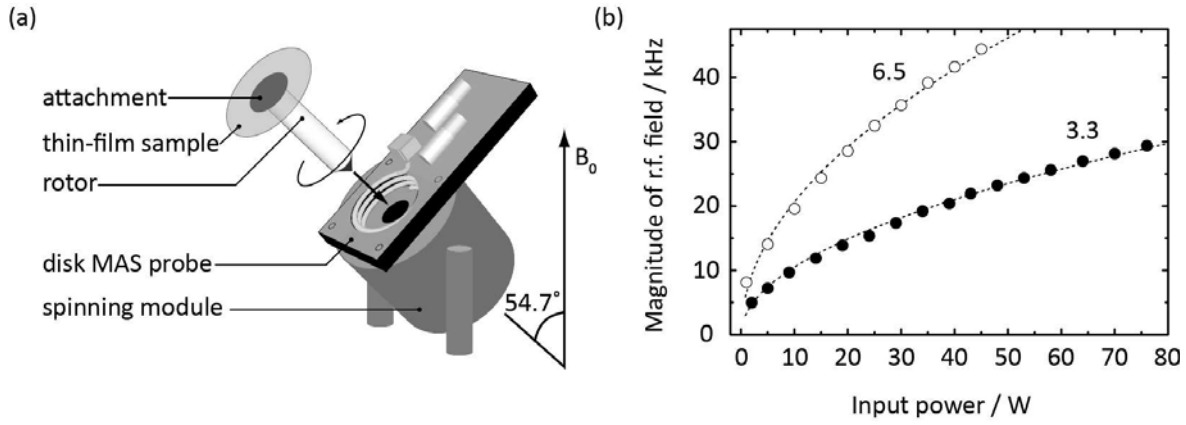

Fig. 1. (a) A schematic description of disk MAS. (b) Input-power dependence of the r.f. field magnitude at 116.4 MHz in the disk MAS probe (filled circles) and a home-built 4mm rotor probe (open circles). The magnitude of r.f. fields was obtained from the ^{7}Li nutation experiments with LiCl aqueous solution. The data points were fitted by a square root function of the form $y = a\sqrt{x}$, and the coefficient a is depicted for each set of the data.

Ex-situ ^{7}Li disk MAS NMR

In order to follow the effects of sequential annealing on the local structure of the $LiCoO_2$ thin films, single pulse NMR and sample annealing were repeated. A 200 nm-thick $LiCoO_2$ thin film was sputtered on a quartz substrate with 12 mm diameter and 0.5 mm thick at room temperature. The number of the ^{7}Li spins contained in the sample was estimated to be 1.1 μmol from the volume of 22.6 nL.

Ex-situ ^{7}Li MAS NMR experiments were performed at 116.4 MHz in 7 T with the disk MAS probe. Spectra were recorded with single-pulse experiments in the spinning at 5 kHz. The pulse width was 8 μs with an input power of 54 W, which corresponds to the r.f. magnitude of 25 kHz. The ^{7}Li FIDs were accumulated over 300000 times with a relaxation delay of 100 ms. The total experimental time was 8.5 hours for each annealing stage.

After the first NMR measurement, the sample was removed from the attachment, then annealed at 400 °C for 3 minutes in a pre-warmed furnace, and cooled in the atmosphere. Then the sample was mounted on the attachment again, and disk MAS NMR was performed in the same experimental conditions. The above steps were repeated until the total annealing time was 18 minutes.

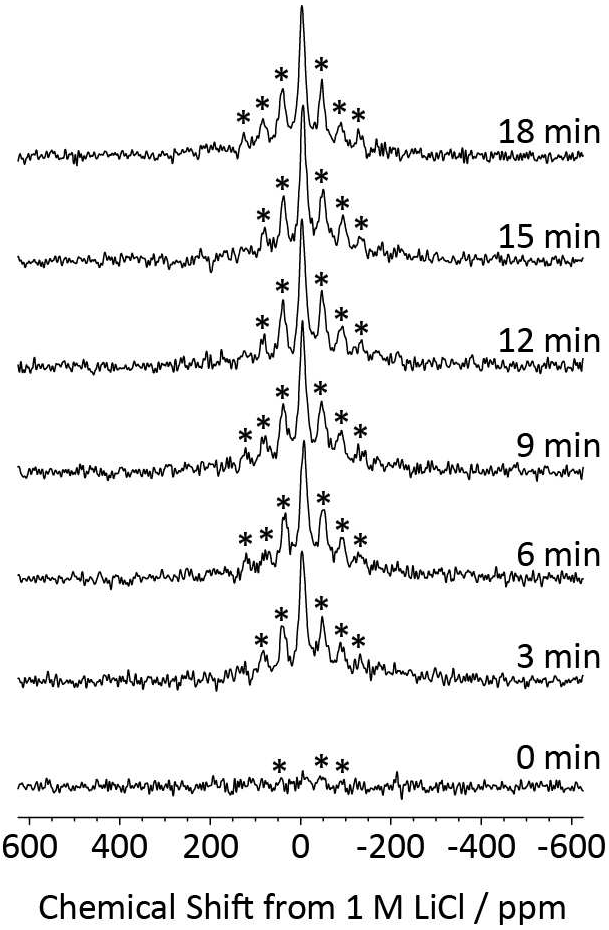

Fig. 2. Ex-situ ^{7}Li disk MAS NMR spectra of an identical 200 nm thick $LiCoO_2$ thin film annealed sequentially at 400°C for 3 minutes. The asterisked peaks are the spinning sidebands.

Fig. 2 shows ex-situ ^{7}Li disk MAS NMR spectra. While the spectrum of non-annealed (as-deposited) sample showed relatively weak signals, a center peak at 0 ppm and a number of spinning sidebands were observed after the first annealing time of 3 minutes. The chemical shift of the center peaks corresponded to that of the $LiCoO_2$ crystal. We found that the line width was much larger than that due to the static field inhomogeneity. This indicates the presence of magnetically nonequivalent ^{7}Li spins.

Considering the similar profile of the spinning side-bands reported in ^{7}Li MAS NMR of $LiCoO_2$ in the paramagnetic state, [18-20] a part of the diamagnetic Co^{3+} ions in the $LiCoO_2$ thin film has presumably changed into paramagnetic Co^{2+} ions, suggesting the existence of oxygen vacancies.

The intensity of the center peak after the first annealing increased by a factor of 7.7. Then the intensity gradually grew as further annealing the sample for up to 18 minutes, as shown in Fig. 3. In a recent report, a $LiCoO_2$ thin film sputtered at room temperature was found to be mostly amorphous, and crystallizes after annealing for 9-15 minutes. [21] The weaker peak intensity of the as-deposited sample could be due to the distribution of the paramagnetic interaction.

The change in the spectra observed in the present work suggests that the as-deposited $LiCoO_2$ thin film in the amorphous phase underwent transition within 3 minutes annealing into the crystalline phase, in which oxygen vacancies remained after the net annealing period of 18 minutes.

Acknowledgment

We appreciate the fruitful discussions with Prof. K. Takegoshi (Kyoto University). This work was financially supported by Core Research of Evolutional Science and Technology of Japan Science and Technology agency (CREST/JST).

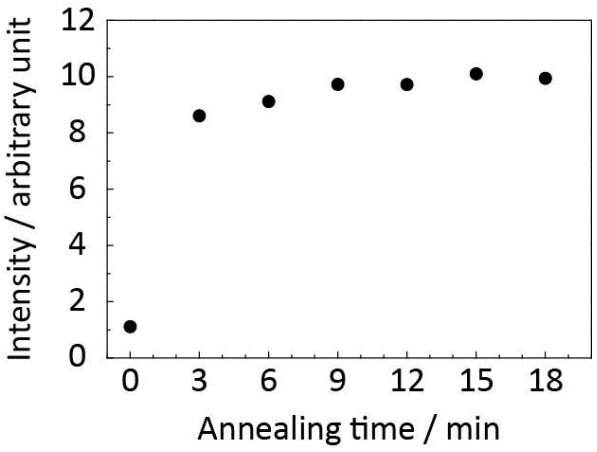

Fig. 3. Annealing-time dependence of the center peak intensity of ^{7}Li disk MAS spectra of the $LiCoO_2$ thin film.

References

[1] J.B. Bates, N.J. Dudney, B. Neudecker, A. Ueda, and C.D. Evans, *Solid State Ionics* **135** (2000) 33-45.
[2] C. P. Grey and N. Dupr, *Chem. Rev.* **104** (2004) 4493-4512.
[3] E. R. Andrew, A. Bradbury, and R. G. Eades, *Nature* **182** (1958) 1659-1659.
[4] E. R. Andrew, A. Bradbury, and R. G. Eades, *Nature* **183** (1959) 1802-1803.
[5] T. M. Alam and H. Y. Fan, *Macromol. Chem. Phys.* **204** (2003) 2023-2030.
[6] K. Landskron, B.D. Hatton, D.D. Perovic, and G.A. Ozin, *Science* **302** (2003) 266-269.
[7] B.D. Hatton, K. Landskron, W. Whitnall, D.D. Perovic, and G.A. Ozin, *Adv. Funct. Mater.* **15** (2005) 823-829.
[8] A. Mazaj, S. Costacurta, N.Z. Logar, G. Mali, N.N. Tusar, P. Innocenzi, L. Malfatti, F. Thibault-Starzyk, H. Amenitsch, V. Kaucic, and G. Soler-Illia, *Langmuir* **24** (2008) 6220-6225.
[9] C.A. Steinbeck, M. Ernst, B.H. Meier, and B.F. Chmelka, *J. Phys. Chem. C* **112** (2008) 2565-2573.
[10] C. Glaubitz and A. Watts, *J. Magn. Reson.* **130** (1998) 305-316.
[11] N.A. Oyler and R. Tycko, *J. Am. Chem. Soc.* **126** (2004) 4478-4479.
[12] D.L. VanderHart, V.M. Prabhu, K.A. Lavery, C.L. Dennis, A.B. Rao, and E.K. Lin, *J. Magn. Reson.* **201** (2009) 100-110.
[13] J.P. Yesinowski, *Phys. Stat. Sol. C* **7** (2005) 2399-2402.
[14] M. Inukai, Y. Noda, and K. Takeda, *Accepted to J. Magn. Reson.*
[15] H. Janssen, A. Brinkmann, E.R.H. van Eck, P.J.M. van Bentum, and A.P.M. Kentgens, *J. Am. Chem. Soc.* **128** (2006) 8722-8723.
[16] K. Yamauchi and T. Asakura, *Chem. Lett.* **35** (2006) 426-427.
[17] M. Inukai and K. Takeda, *Concepts Magn. Reson. B* **33** (2008) 115-123.
[18] M. Menetrier, Y. Shao-Horn, A. Wattiaux, L. Fournes, and C. Delmas, *Chem. Mater.* **17** (2005) 4653-4659.
[19] K. Nakamura, H. Hirano, D. Nishioka, S. Endou, K. Itsuki, Y. Michihiro, T. Moriga, N. Kuwata, and J. Kawamura, *Solid State Ionics* **180** (2009) 621-625.
[20] M.P.J. Peeters, M.J. van Bommel, P. Wolde, H.A.M. van Hal, W.C. Keur, and A.P.M. Kentgens, *Solid State Ionics* **112** (1998) 41-52.
[21] H.Y. Park, S.C. Nam, Y.C. Lim, K.G. Choi, K.C. Lee, G.B. Park, J.B. Kim, H.P. Kim, and S.B. Cho, *Electrochim. Acta* **52** (2007) 2062-2067.

P-116 Study of phase structures in metal deuterides using two-dimensional one pulse spectroscopy

You Suzuki and Shigenobu Hayashi
National Institute of Advanced Industrial Science and Technology (AIST)

[Introduction]

Magic-angle-spinning (MAS) is used in many investigations to enhance spectral resolutions and sensitivity in solid-state NMR. Two-dimensional one pulse (TOP) spectroscopy is one of the methods to enhance the resolution furthermore. In this method, a 1D MAS NMR spectrum is represented in a 2D resolved fashion.

Vanadium metal can absorb a large amount of hydrogen to the extent of a hydrogen-to-metal atomic ratio of 2. The structures and phase diagrams of vanadium hydrides have extensively been studied so far, including vanadium deuterides. The vanadium crystal structure and the hydrogen (deuterium) site are dependent on the [H]/[V] and temperature. At room temperature, there are two structures in the range $0 < [H]/[V] < 1$. At a low hydrogen (deuterium) content, vanadium hydrides and deuterides have a body-centered-cubic (BCC) structure. Around $[H]/[V] = 0.5$ the BCC structure changes into a body-centered-tetragonal (BCT) structure. In the region $0.5 < [H]/[V] < 1$, structures of hydrides and deuterides are not coincident. It is known that vanadium deuterides have a BCC structure while vanadium hydrides still remain the BCT structure. It is already known where hydrogen and deuterium are located. Hydrogen and deuterium are located at an octahedral site in the vanadium BCT lattice, and at a tetrahedral site in BCC. Hydrogen in a tetrahedral site has higher mobility than in an octahedral site. Therefore, the NMR peak for the BCC structure become sharper than that for BCT. $Ti_{0.1}V_{0.9}H_xD_y$ has been studied using DSC, XRD and static NMR. The crystal structures of metal atoms resemble vanadium hydride or deuteride. $Ti_{0.1}V_{0.9}H_{0.77}$ has a BCT structure, and $Ti_{0.1}V_{0.9}D_{0.73}$ has a BCC structure.

In this study, we have applied TOP spectroscopy to ^2H MAS NMR spectra of vanadium deuterides and $Ti_{0.1}V_{0.9}H_xD_y$ constructed with several components with different structures, and we have tried separation of the components and have determined shifts of minor components.

Sample	Crystal structure
$VD_{0.50}$	BCT BCC*
$VD_{0.57}$	BCT* BCC
$Ti_{0.1}V_{0.9}H_{0.77}$	BCT
$Ti_{0.1}V_{0.9}H_{0.5}D_{0.2}$	BCT BCC*
$Ti_{0.1}V_{0.9}H_{0.2}D_{0.5}$	BCT* BCC
$Ti_{0.1}V_{0.9}D_{0.73}$	BCC

Table 1. The structure of vanadium deuterides and $Ti_{0.1}V_{0.9}H_xD_y$
* a small amount

[Experimental]

Vanadium metal powder (325 mesh, 99.5% min) was obtained from Mitsuwa Pure Chemicals. Vanadium deuterides were obtained by direct reaction between vanadium metal and D_2 gas. The deuterium content was determined from the absorbed gas volume.

Titanium powder (purity, 99.9%) and vanadium powder (99.9%) were purchased from Soekawa Chemicals and High Purity Chemicals, respectively. The binary alloys $Ti_{0.1}V_{0.9}$ were prepared by arc melting of the appropriate mixture of Ti and V

TOP spectroscopy, metal deuteride, metal hydride

powders under an argon atmosphere. $Ti_{0.1}V_{0.9}H_{0.77}$ and $Ti_{0.1}V_{0.9}D_{0.73}$ were obtained by direct reaction of the$Ti_{0.1}V_{0.9}$ alloy with H_2 or D_2 gas. $Ti_{0.1}V_{0.9}H_{0.2}D_{0.5}$ and $Ti_{0.1}V_{0.9}H_{0.5}D_{0.2}$ were prepared by mixing two of the parent samples in required ratios and homogenizing the mixture inside a closed chamber at 533 K for a week.

All NMR spectra were obtained using Bruker ASX400 spectrometer at room temperature. ^2H MAS NMR spectra were measured by single pulse with 10~15 kHz magic angle spinning. TOP spectra were processed by a home-made program. For vanadium deuterides, the FIDs were expanded to two dimensional FIDs by excluding the first one point for each step. For $Ti_{0.1}V_{0.9}H_xD_y$, the FIDs were processed in a similar manner to vanadium deuterides, and the shifting process was synchronized with the MAS rotation.

[Results]

^2H MAS NMR spectra of $VD_{0.50}$ are shown in Figure 1(A). There were two isotropic peaks assigned to BCT and BCC in the spectrum of $VD_{0.50}$. The BCT peak has several spinning sidebands (SSBs). A TOP spectrum of the SSB region for $VD_{0.50}$ is shown in Figure 2(A). In the ^2H MAS NMR spectrum of $VD_{0.50}$ (Figure 1(A)), there are two peaks, and the sharp BCC peak seems to have no SSBs. However, in the TOP spectra (Figure 2(A)), sharp SSB peaks are observed on the broad BCT SSBs.

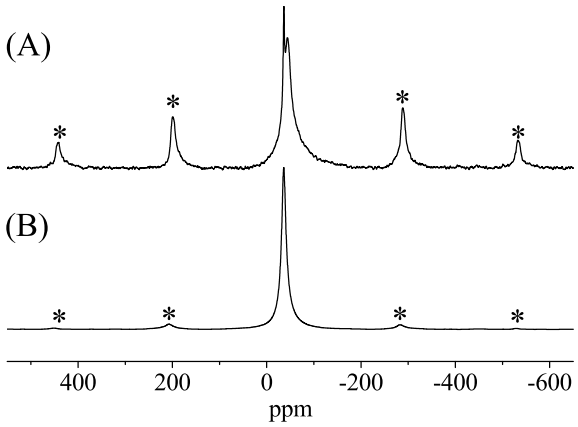

Figure 1. ^2H MAS NMR spectra of (A) $VD_{0.50}$ and (B) $VD_{0.57}$ with 15 kHz spinning. The marks * indicate SSBs.

In the spectrum of $VD_{0.57}$ shown in Figure 1(B), the sharp peak comes from a tetrahedral site in the BCC lattice and very weak SSBs are observed. In the TOP spectra (Figure 2(B)), there are broad SSBs under the sharp SSBs. The sharp SSBs should come from the BCC peak, and the broad SSBs would come from the BCT peak which is not observed clearly in the 1D ^2H MAS NMR spectrum. The shift values of SSBs of the BCT peak are -282 and 201 ppm. From these values, the shift of the BCT central peak will be -40.5 ppm.

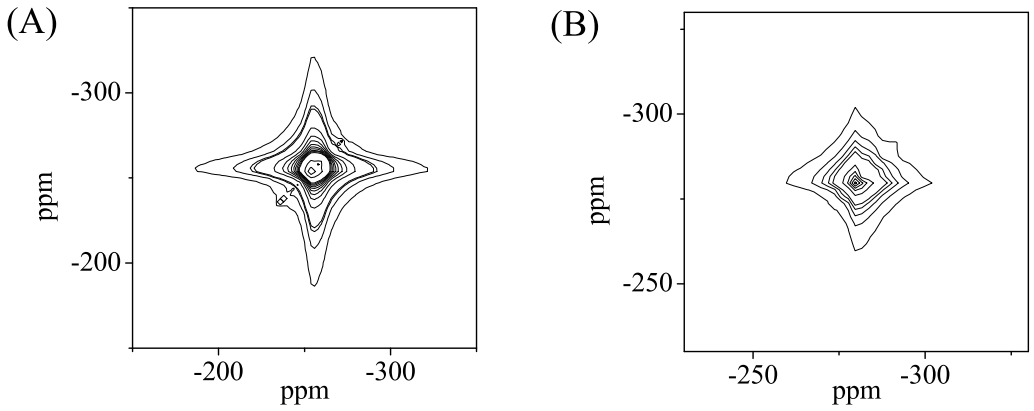

Figure 2. TOP spectra of the SSB region for (A) $VD_{0.50}$ and (B) $VD_{0.57}$.

P-117 Solid-state NMR analysis of molecular orientations in organic light-emitting diodes

Masashi Fukuchi, Tatsuya Fukushima, and Hironori Kaji
Institute for Chemical Research, Kyoto University

In this study, we characterize the molecular orientations in amorphous thin films of phosphine oxide derivatives, which have excellent electron transport properties, by solid-state NMR. We reveal a clear correlation between the device performances and the molecular orientations.

[Introduction]

Molecular orientations of materials in organic devices are considered crucial to understand the device performances. However, the materials in organic light-emitting diodes and organic solar cells are in amorphous states in most cases, and the sample amounts in these devices are significantly limited. Therefore, the characterization of the molecular orientations has been difficult so far. Under such circumstances, we have recently started the solid-state NMR analysis, which provides detailed structural information, even for materials in amorphous states. In this study, we carried out chemical shift anisotropy (CSA) measurements on solid-state NMR to reveal molecular orientations of $POPy_2$ and Tp4PyPhO (see Fig. 1 for the chemical structures) in amorphous thin films. The carrier mobility of these materials, which have excellent electron transport properties, depends on the device fabrication conditions and the correlation between the carrier mobility and the molecular orientations is clarified.

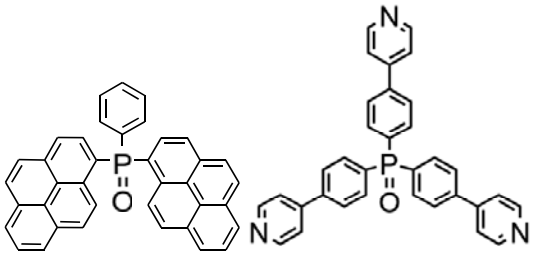

Fig. 1. Chemical structures of $POPy_2$ and Tp4PyPhO.

[Experimental]

$POPy_2$ vacuum-deposited devices were fabricated at the deposition rates of 0.1, 1.0, and 4.0 nm/s. From the devices and the time-of-flight measurements, we found that the electron mobility became higher as the deposition rate increased. To understand the change of the electron mobility, CSA measurements were carried out for $POPy_2$ thin films (200 nm) at the above three deposition rates. More than 100 sheets of thin films were stacked to enhance the signal-to-noise ratio and inserted into a NMR coil with the normal vector of the films parallel to $\boldsymbol{B}_0$. The CSA measurements with CP preparation, ^{1}H TPPM dipolar decoupling, and Hahn-echo were carried out at 300 K on a Bruker 400 MHz AVANCE III spectrometer and a double resonance 7.5 mm static probe was used. Similarly for Tp4PyPhO, the electron mobility became higher as the deposition rate increased, and the CSA measurements were carried out under the same experimental condition as above. The deposition rates were 0.05 and 0.5 nm/s for Tp4PyPhO.

Solid-state NMR, Chemical shift anisotropy, Molecular orientation, Organic light-emitting diodes

[Results and discussion]

Fig. 2 shows the ^{31}P CSA spectra of $POPy_2$ in the thin films at different deposition rates. The spectrum for random orientation is also shown for reference. The chemical shift, σ, depends on the molecular orientation;

$$\sigma = \sigma_{\perp} \sin^2\theta + \sigma_{//} \cos^2\theta$$

where θ is the angle between P=O and $\boldsymbol{B_0}$. For example, the signal at around 100 ppm corresponds to the molecular orientation of P=O perpendicular to $\boldsymbol{B_0}$. The signal at around -100 ppm corresponds to the molecular orientation of P=O parallel to $\boldsymbol{B_0}$. The CSA spectra for the vacuum-deposited thin films in Fig. 2 clearly show that $POPy_2$ molecules were not in completely random orientation but in an oriented state with the P=O direction tending to be perpendicular to the substrate, even for the lowest deposition rate in this study, 0.1 nm/s. As the deposition rate increased further, a narrower distribution of the molecular orientations was found.

Fig. 3 shows the ^{31}P CSA spectra of Tp4PyPhO in the thin films at different deposition rates and in randomly orientated state. Similarly to the case of $POPy_2$, P=O vector in Tp4PyPhO tended to orient perpendicular to the substrate.

From the above solid-state NMR experiments, the orientation of these molecules was found to become higher with increasing the deposition rate, and the molecular orientation is considered to be the origin of the increase of the carrier mobility.

[Acknowledgement]

This research is granted by the Japan Society for the Promotion of Science (JSPS) through the "Funding Program for World-Leading Innovative R&D on Science and Technology (FIRST Program)," initiated by the Council for Science and Technology Policy (CSTP).

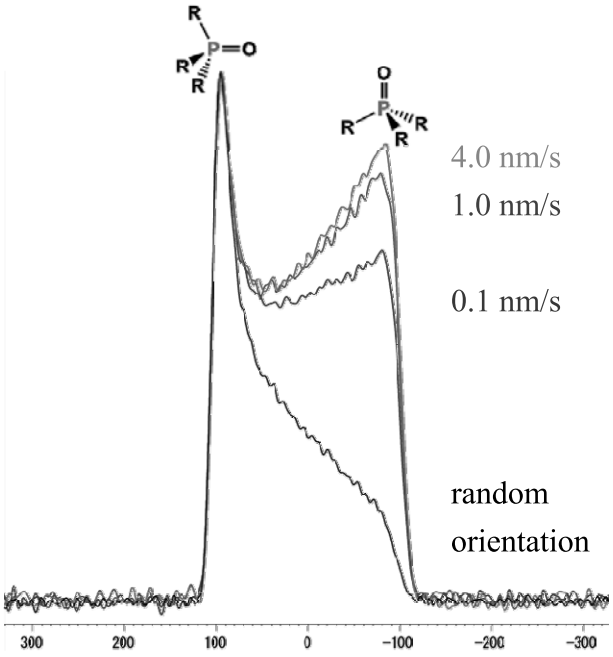

Fig. 2. ^{31}P CSA spectra of $POPy_2$ in the vacuum-deposited thin films at the deposition rates of 0.1, 1.0, and 4.0 nm/s. The spectrum for random orientation is also shown for reference.

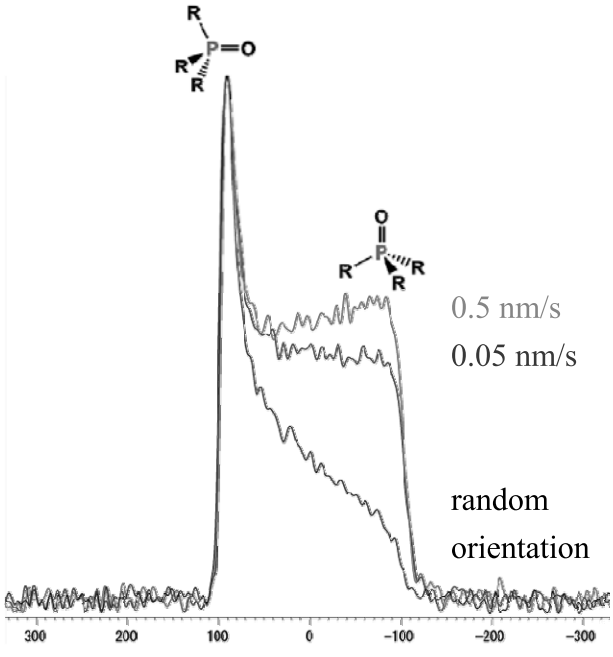

Fig. 3. ^{31}P CSA spectra of Tp4PyPhO in the vacuum-deposited thin films at the deposition rates of 0.05 and 0.5 nm/s. The spectrum for random orientation is also shown for reference.

P-118 Solid-State NMR Study of Molecular Dynamics of Imidazole Related to Proton Conductivity

Tsuyoshi Umiyama, Ryutaro Ohashi, Tomonori Ida, Motohiro Mizuno
Department of Chemistry, Graduate School of Natural Science and Technology, Kanazawa University, kanazawa, 920-1192, Japan

Abstract: The development of proton-conductive materials using imidazole has attracted considerable attention. Imidazolium salts and polymers with imidazole are known to show high proton conductivity. Motions of imidazole molecules are considered to play important role in the proton conductivity. However, detailed information of molecular motion of imidazole in these high proton conductive materials has not been obtained.

In the present study, we analyzed the mode and rate of molecular motions of imidazole in imidazolium succinate and pol(vinylphosphonic acid) with imidazole which show high proton conductivity using solid-state ^{2}H NMR.

Introduction: The development of proton-conductive materials using imidazole has attracted considerable attention. For example, imidazolium salts of dicarboxylic acids display high conductivity (range of 10^{-7}-10^{-5} S m^{-1}) [1] between 293 and 473 K. Fig. 1 shows the crystal structure of imidazolium succinates which is one of imidazolium salts of dicarboxylic acids. This crystal forms layers along a-axis. In the layer, the chains of the acid's molecules are bonded by strong hydrogen bonds O−H···O. Also the succinate anions create the second type N−H···O hydrogen bonds with the imidazolium cations. It seems that the high proton conductivity comes from the reorientation of the imidazole ring (Grotthus mechanism). In this study we measured the ^{2}H solid-state NMR spectrum and spin-lattice relaxation time T_1 of imidazolium succinate in order to investigate the dynamics of imidazole molecular and to clarify the mechanism of high proton conductivity of imidazolium succinate.

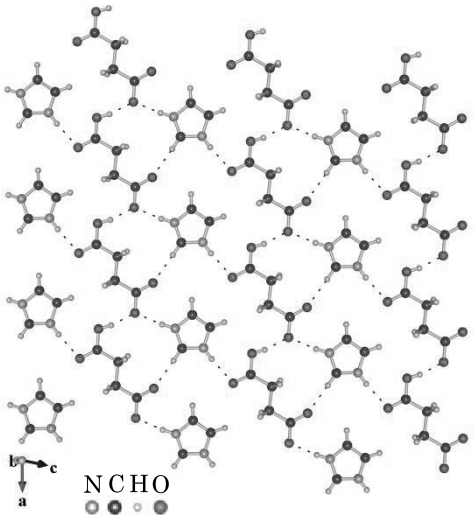

Fig. 1. Crystal structure of imidazolium succinate[1], [2].

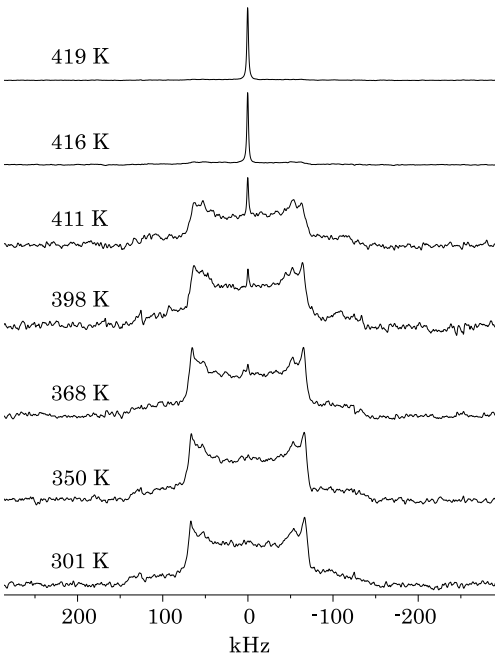

Fig. 2. ^{2}H solid-state NMR spectra.

Experimental: The ^{2}H solid-state NMR spectrum was measured by an ECA 300 spectrometer at ^{2}H frequencies of 45.282 MHz. T_1 were determined by the saturation recovery method. Imidazolium succinate is synthesized by Imidazole-4d (approximately 98% pure, CIL)and succinate asid (approximately 99.5% pure, Wako).

^{2}H NMR, Proton-conductivity, Imidazole

Results and discussion: The temperature dependence of the ^{2}H NMR spectrum for imidazolium succinate is shown in fig. 2. The spectrum revealed broad Pake-pattern between 301 and 368 K. The sharp component around 0 kHz was observed above 398 K. The intensity of sharp component increased with increasing temperature. The remarkable change in the line shape of broad component was not observed.

The experimental and calculated ^{2}H solid-state NMR spectra of imidazoluim succinate at 301, 411 K are shown in fig. 3. From the line shape of broad spectrum, the quadrupole coupling constant e^2qQ/h and the asymmetry parameter η were estimated as 170 kHz and 0, respectively.

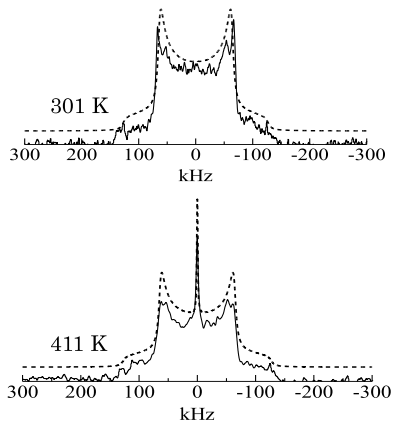

Fig. 3. Observed and calculated ^{2}H solid-state NMR spectra.

The temperature dependence of the area intensity of the spectrum is shown in fig. 4. Here, the intensity was normalized using the spectrum at 332 K. The intensity of sharp component increased suddenly near melting point (418 K). On the contrary the intensity of broad component and the total area intensity decreased with increasing temperature above 380 K. These phenomena are predicted to be caused by the molecular motion of the imidazole with the jumping rate of 10^3~10^4 Hz.

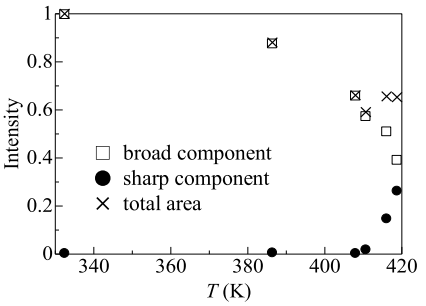

Fig. 4. Temperature dependence of spectral intensity.

Fig. 5 shows the temperature dependence of T_1 of the broad component. At room temperature, T_1 was on the order of 100 s. T_1 decreased exponentially with increasing temperature and became 1.2 s at 411 K. Assuming that the relaxation of the broad component is dominated by the 180° flip of imidazole molecule, the jumping rate was estimated as 10^4 Hz from the T_1 value at 411 K. The obtained jumping rate is consistent with the results of the spectral intensity. The activation energy of the 180° flip of imidazole molecule was estimated as 42 kJ/mol from the slope of the temperature dependence of T_1.

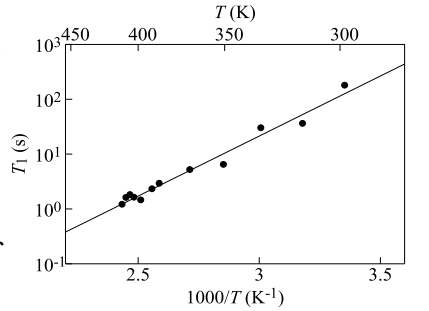

Fig. 5. Temperature dependence of T_1 of broad component

The temperature dependence of T_1 for the sharp component is shown in fig. 6. T_1 increased exponentially with increasing temperature. The activation energy of the isotropic rotation of imidazole molecule was estimated as 59 kJ/mol.

Thus, the high proton conductivity of imidazolium succinate crystal is considered to be related to both slow 180° flip and rapid isotropic rotation of imidazole molecules.

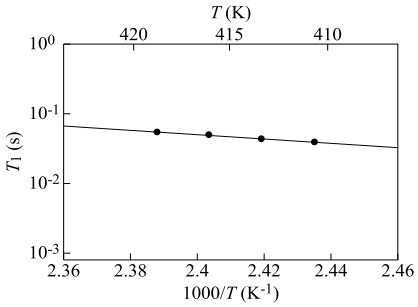

Fig. 6. Temperature dependence of T_1 of sharp component.

Reference

[1] K. Pogorzelec-Glaser, Cz. Pawlaczyk, A. Pietraszko, E. Markiewicz, J. Pow. Sou., 173 (2007), 800-805.

[2] K. Momma and F. Izumi, J. Appl. Crystallogr., 41 (2008), 653-658.

P-119 Pulsed NMR Evaluation on Curing Process of Epoxy Resin and Thermal Behavior of Cured Resin

Takuzo Kurotsu, Atsushi Asano, Hiroki Kimoto and Chikako Nakazawa
Department of Applied Chemistry, National Defense Academy.

ABSTRACT

A curing process of epoxy resin was studied by pulsed NMR method in terms of mobility of proton. As the curing reaction proceeds, three kinds of spin-spin relaxation time(T_{2L}(long), T_{2S}(short) and T_{2M}(intermediate)) were obtained from the observed solid echo train signals. A short T_{2S} below 20us suggests an existence of a motion restricted chain, that is, cured element of resin and its fraction of T_{2s}:(F_S) increased sigmoidally with its reaction time. On the other hand, the fractions of T_{2L}; F_L decreased with time reciprocally, suggesting the disappearance of highly mobile molecules arose from pre-cured resin. These results mean that the curing process reflects on the time course of relaxation times and their fractions.

INTRODUCTION

Pulsed NMR method can generally used to elucidate certain aspects of polymer structure and molecular motion. Spin-lattice relaxation time, T_1, and spin-spin relaxation time, T_2, are parameters sensitive to the behaviour of molecular motion, such as a chain entanglement or the permanent cross-links of polymer. The entanglement of polymer chain which appears like in a curing process of epoxy resin, restrict chain mobility since the resin reacts with the curing agent to form a permanent network structure by chemical bonding between them. In this work, we demonstrate that pulsed NMR is sufficiently sensitive to the changes in the material properties of epoxy resin and could be used for a non-destructive state assessment of the curing process.

EXPERIMENTAL

Epoxy Resin (Seiwa Pro Co. Ltd) was used for measurements. The same volumes of (0.2ml) of pre-cured epoxy resin and curing agent were mixed with a platinum wire in a 15mm-lengthe glass tube (6mmϕ) for 1min. After that the tube was put into an NMR sample tube (10mmϕ) and then solid echo signal was recorded at probe temperature (25C). NMR measurements were carried out with a JEOLMu25 spectrometer operating at a frequency of 25MHz.

RESULTS AND DISCUSSION

As the curing reaction proceeds, the resin becomes highly viscous, and can be solidified within100 min. Solid echo signals in the curing process can be fitted to a sum of Weibull function, and three kinds of relaxation times (T_{2S} (short), T_{2L} (long) and T_{2M} (intermediate)) were obtained by following equations:

$$S(t)= S_{0i}\,\Sigma exp[-(t/T_2)^{Ei}] \qquad (1)$$

Here, E_i is the Weibull coefficient , S_{0i}, the signal intensity of the *i-th* component at t=0, T_2 of the *i-th* component (F_i) with given by

$$F_i=S_{0i}/\Sigma S_{0i} \qquad (2)$$

The Weibull coefficient be taken as having either a Gaussian($E=2$), exponential ($E=1$) or intermediate($1<E<2$).

Pulsed NMR, Epoxy resin, Network structure

These relaxation times gradually decreased with reaction time. Figure 1 shows a change in each fraction of T_{2S}, T_{2M} and T_{2L} components, referred to these as F_S, F_M, F_L, respectively against the reaction time. F_L decreased monotonously from 80% to a few percents. This component is the most mobile species among three fractions, and corresponds to the amounts of un-cured epoxy resin and/or the curing agent. P_S, of which relaxation time varied from 50 to 20 us, increased sigmoidally to reach almost 80% after a reaction time of 60min. Taking into an account of value for T_{2S} and its increasing tendency, F_S is attributable to the amounts of the motion restricted cured-resin. P_M, of which relaxation time varies from 200 to 60 μs, gradually increased and then showed a decreasing tendency around at reaction time of 10 min. The molecular motional region belonging to F_L transits into that of F_S, via F_M. The change from an increasing to a decreasing tendency in F_M, therefore, indicates an occurrence of an autocatalytic gel effect in this reaction. These kinetic behaviors of the components were also observed in a bulk polymerization where a gel effect generally occurs. *Ps* observed in the polymerization is associated with an existence of polymer chain entanglements of which the motion is severely restricted (20μs). The time course of those three components, therefore, explains in regards to the proton motion how the curing process accompanied with a gel effect proceeds to form three dimensional polymer chain networks. T_1 was also observed during the reaction, since this parameter exhibits different sensitivity to molecular motion at a rate of Larmer frequency and in kHz range. The time course of this parameter showed a linear increase tendency against the reaction time, suggesting that there exists a network structure in the cured resin. Therefore, those results make it possible to perform a non-destructive monitoring the curing reaction process in real time, and to substantiate an assessment of a cross-linking polymer on the laboratory reference data. Thermal stability of the cured resin was also studied. Figure 2 shows that initial signal intensity(I) began to decrease from 373K, which suggests the decomposition begins to occur at the temperature, since the initial value of the signal is proportional to the proton content in the cured resin.

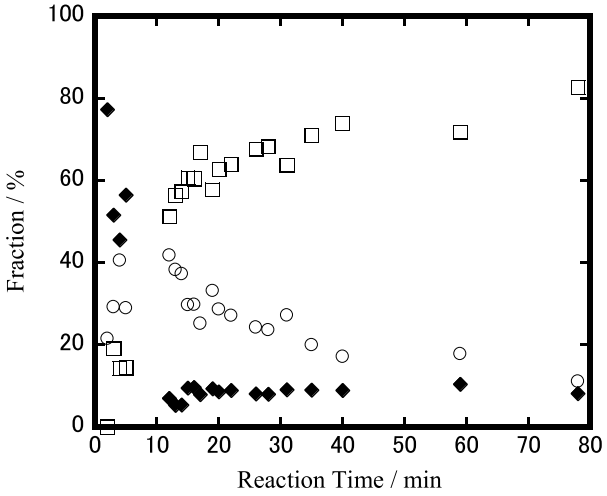

Fig. 1. F_S, F_M, F_L *vs* reaction time.
□; F_S, ○; F_M, ◆; F_L

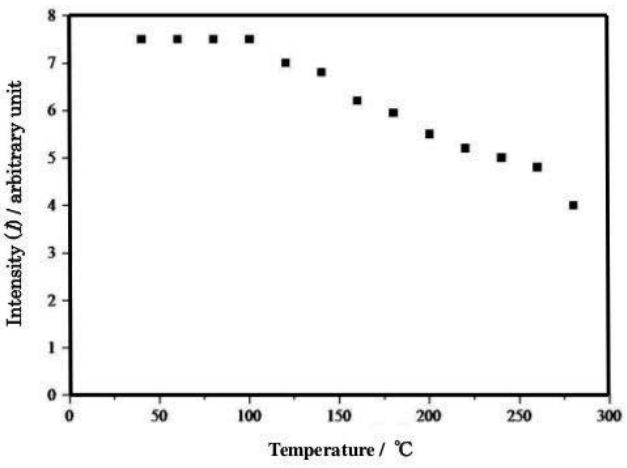

Fig. 2. Temperature dependence of the initial intensity of solid echo signal

P-120 Dynamics of water molecules in mesoporous silica SBA-15 as studied by ^{2}H NMR

Tatsuya Miyatou[1], Kouichi Sazanami[1], Ryutaro Ohashi[1], Motohiro Mizuno[1] and Shigeharu Kittaka[2]
[1]Department of Chemistry, Graduate School of Natural Science and Technology, Kanazawa University and
[2]Department of Chemistry, Faculty of Science, Okayama University of Science.

ABSTRACT

SBA-15 has one-dimensional honeycomb mesopore and micropore connecting these mesopore. Two thermal anomaly is observed by DSC mesurement on cooling process. One is freeze of water in mesopore, and another is freeze of water in micropore. Dynamics of water molecules in the mesopore and micropore can be influenced a great deal by interaction with silica surface and confinement effect. By using ^{2}H NMR, dynamics of these water molecules was studied. Heavy water in SBA-15 with varied pore size was measured of ^{2}H NMR spectrum and spin-lattice relaxation time.

INTRODUCTION

SBA-15 is mesoporous silica which has one-dimensional honeycomb mesopore. Fig. 1 shows structure of SBA-15. Size of mesopore is adaptable around 10 nm in diameter. SBA-15 is expected to use as catalyst and adsorptive medium.

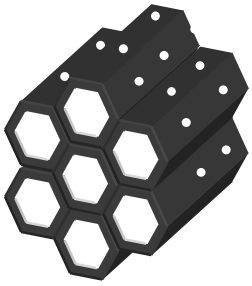

Fig. 1 Structure of mesoporous silica SBA-15.

So far, water molecules in SBA-15 was investigated by differential scanning calorimetry (DSC) [1, 2]. Two thermal anomalies are observed from the DSC measurement in the cooling process except freeze of excess water. One is an exothermic peak due to freezing of water in cylindrical mesopore at 250-260 K. Another is a small exothermic peak at 230 K. SBA-15 has the micropore interconnecting mesopore in addition to the principal mesopore [3]. Although the thermal anomaly at 230 K is considered to be connected with freeze of water in micropore of SBA-15, details have not been disclosed.

Therefore, it is important to study on dynamics and structure of waters in SBA-15. In this paper, the dynamics of water molecules in these micropore and principal mesopore of SBA-15 is studied by measuring the ^{2}H NMR spectrum and spin-lattice relaxation time (T_1).

EXPERIMENTAL

SBA-15 samples with varied pore size were prepared following an original technique reported by Zhao et al [4]. Principal pore of SBA-15 is 7.1 nm and 10.4 nm in diameter. Heavy water was introduced to pore of SBA-15 and excess heavy water existed around SBA-15 powders. The ^{2}H NMR measurements were conducted in a JEOL ECA 300 spectrometer with 45.282 MHz frequency. The ^{2}H NMR spectra were measured by using a quadruple echo sequence $(90°)_x$-τ-$(90°)_y$-τ-acquisition. ^{2}H NMR T_1 was measured by the inversion recovery method.

Mesoporous silica, Confinement effect, Molecular dynamics

RESULTS AND DISCUSSION

Fig. 2 shows ^{2}H NMR spectrum of heavy water in SBA-15(10.4 nm). In these spectra, ^{2}H NMR signal of bulk ice was removed by saturation (repetition time 1 s). The spectrum consists of sharp component and broad one. Broad component comes from static water molecules and sharp component comes from water rotating faster than quadrupole interaction (about 200 kHz). In fig. 2, the broken line shows the calculated spectrum of broad component. The line shape of sharp component was fitted by Lorentz curve. In the cooling process, the spectrum of sharp component consists of two Lorentz curves (Sharp 1, Sharp 2) at 260-230 K. Sharp 1 was defined as the major component. Fig. 3(a) shows the temperature dependence of the signal intensity of sharp and broad components. The signal intensity is normalized by intensity at 268 K. The intensity of Sharp 1 deceased with decreasing temperature and disappeared at 200 K. The intensity of Sharp 2 was much lower than that of Sharp 1. Sharp 1 and Sharp 2 are corresponding to the water in micropore or surface water in principal mesopore, since waters of principal mesopore freeze below 260 K. The surface water of mesopore is probably more than water in micropore. Therefore, Sharp 1 and Sharp 2 can be assigned the surface water and micropore water, respectively. The intensity of broad component decreased below 230 K, since the T_1 of broad component became longer than repetition time of the NMR measurements. Fig. 3(b) shows the temperature dependence of full width half maximum (FWHM) of sharp components. The FWHM value of Sharp 1 became larger than that of Sharp 2. This result indicates that the surface water is bound down more strongly than micropore water.

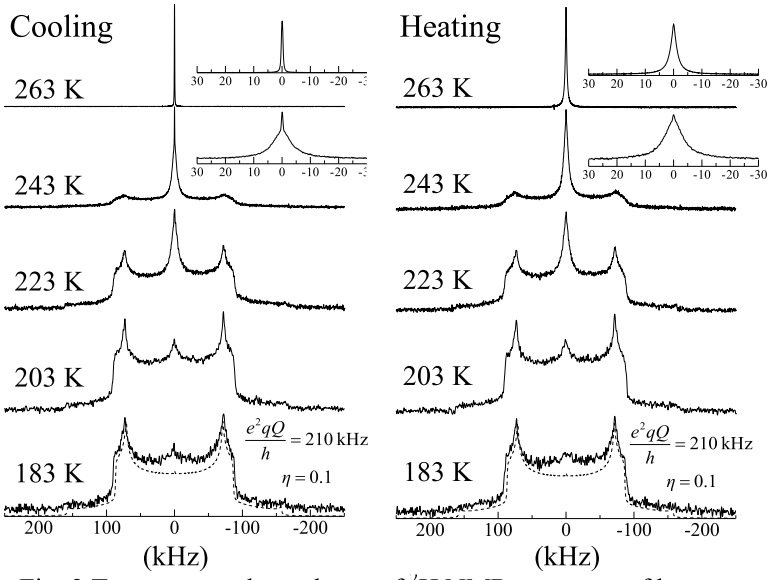

Fig. 2 Temperature dependence of ^{2}H NMR spectrum of heavy water in SBA-15(10.4 nm).

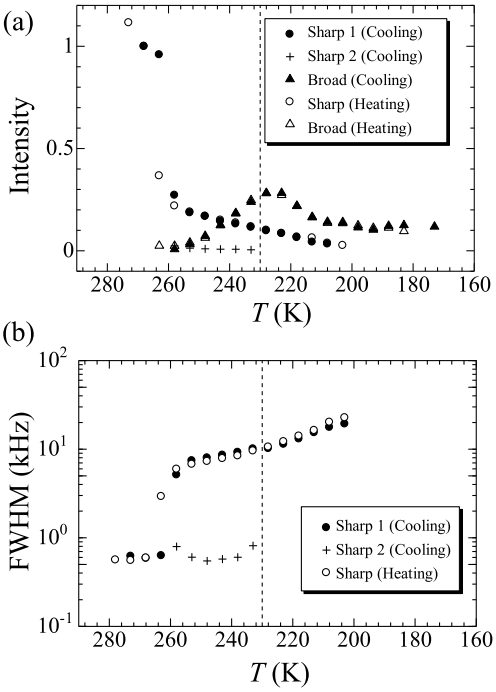

Fig. 3 Temperature dependence of (a) signal intensity and (b) full width half maximum (FWHM) of sharp and broad components in ^{2}H NMR spectrum of SBA-15(10.4 nm).

REFERENCES

[1] A. Schreiber, I. Ketelsen and G. H. Findenegg, *Phys. Chem. Chem. Phys.* **3**, 1185(2001).

[2] S. Kittaka, Y. Ueda, F. Fujisaki, T. Iiyama and T. Yamaguchi, *Phys. Chem. Chem. Phys.* on the website.

[3] A. Galarneau, H. Cambon, F. D. Renzo, R. Ryoo, M. Choi and F. Fajula, *New J. Chem.* **27**, 73(2003).

[4] D. Y. Zhao, J. L. Feng, Q. S. Huo, N. Melosh, G. H. Fredrickson, B.F. Chmelka and G. D. Stucky, *Science* **279**, 548(1998).